A mechanics-based perspective on the function of the esophagogastric junction during functional luminal imaging probe manometry

Guy Elisha[1], Sourav Halder[2], Shashank Acharya[1], Dustin A. Carlson[3], Wenjun Kou[3], Peter J. Kahrilas[3], John E. Pandolfino[3], and Neelesh A. Patankar*[1,2]

[1]Department of Mechanical Engineering, McCormick School of Engineering, Northwestern University Technological Institute, 2145 Sheridan Road, Evanston, IL 60201

[2]Theoretical and Applied Mechanics Program, McCormick School of Engineering, Northwestern University Technological Institute, 2145 Sheridan Road, Evanston, IL 60201

[3]Division of Gastroenterology and Hepatology, Feinberg School of Medicine, Northwestern University, 676 North St. Clair Street, Arkes Suite 2330, Chicago, IL 60611

Abstract

The esophagogastric junction (EGJ) is located at the distal end of the esophagus and acts as a valve allowing swallowed food to enter the stomach and preventing acid reflux. Irregular weakening or stiffening of the EGJ muscles results in changes to its opening and closing patterns which can progress into esophageal disorders. Therefore, understanding the physics of the opening and closing cycle of the EGJ can provide mechanistic insights into its function and can help identify the underlying conditions that cause its dysfunction. Using clinical functional lumen imaging probe (FLIP) data, we plotted the pressure-cross-sectional area loops at the EGJ location and distinguished two major loop types – a pressure dominant loop (PDL) and a tone dominant loop (TDL). In this study, we aimed to identify the key characteristics that define each loop type and determine what causes the inversion from one loop to another. To do so, the clinical observations are reproduced using 1D simulations of flow inside a FLIP device located in the esophagus, and the work done by the EGJ wall over time is calculated. This work is decomposed into active and passive components, which reveal the competing mechanisms that dictate the loop type. These mechanisms are esophagus stiffness, fluid viscosity, and the EGJ relaxation pattern.

Keywords: esophagus, esophagogastric junction, elastic tube flow, peristalsis, reduced-order model, pressure-area hysteresis, functional lumen imaging probe

1 Introduction

The esophagus is a tubular organ responsible for transferring swallowed food to the stomach by using a peristaltic contraction wave (muscle contraction) (Mittal, 2016). The esophagogastric junction (EGJ) is the region at the junction of the esophagus and the stomach, which includes a neurally controlled sphincter (the lower esophageal sphincter or LES) and the surrounding musculature. It is an important component of the digestive track, as it controls the entry of food into the stomach while preventing gastric acid from entering the esophagus (Mittal and Balaban, 1997).

The degradation of the muscles at the EGJ can result in a more compliant EGJ, causing acid reflux (Pandolfino et al., 2003; Kwiatek et al., 2010). Reflux, caused by some degree of uncontrolled opening of

*Corresponding author: N. A. Patankar (n-patankar@northwestern.edu)

the EGJ, can lead to symptoms such as heartburn, regurgitation, chest pain, dysphagia or mucosal damage (esophagitis), all within the spectrum of gastroesophageal reflux disease (GERD) (Pandolfino et al., 2003; Kahrilas, 2008). It has been reported that GERD is the most common gastrointestinal diagnosis during doctors' office visits, and that 14-20% of the adult population in the United States suffers from some degree of GERD (Kahrilas, 2008; Shaheen et al., 2010). On the other hand, diseases such as achalasia are characterized by a lack of peristalsis and an absence of EGJ relaxation which restricts EGJ opening and emptying of the esophagus, causing profound dysphagia (Boeckxstaens et al., 2014; Eckardt and Eckardt, 2009). Therefore, understanding the physics of the opening and closing of the EGJ can provide a mechanistic insight into its functions and can help identify the underlying conditions that cause its dysfunction.

One approach to study the opening and closing pattern of the EGJ is by tracking its pressure and cross-sectional area over time. Plotting pressure vs. volume hysteresis is common in cardiovascular studies (Gregersen and Lo, 2018). Additionally, pressure vs. cross-sectional area plots have been previously used to investigate the anal sphincter (Zifan et al., 2019) and the upper esophageal sphincter (Omari et al., 2015, 2016). However, a similar analysis has never been taken to study the EGJ.

The functional luminal imaging probe (FLIP) can be used to evaluate the state of the EGJ. It is unique as it allows distensibility testing as well as simultaneously tracking pressure and cross-sectional area. The device is composed of a catheter surrounded by a cylindrical shaped bag that measures the cross-sectional area of the esophagus at 16 adjacent locations and pressure at one distal location as a function of time (Carlson et al., 2015, 2016). The FLIP is inserted into the esophagus and placed within the esophageal lumen, bypassing the EGJ. The FLIP bag is incrementally inflated with fluid and the esophageal wall responds to it with a distinctive pattern presented in figure 1. The esophageal wall muscle contract in a peristaltic fashion, pushing fluid towards the distal end of the esophagus. As a result of the moving contraction, the pressure at the distal end of the FLIP bag increases. In parallel to the propelling contraction wave, the initially contracted EGJ relaxes and opens. At the end of the contraction cycle, the muscle contraction wave merges with the EGJ, causing it to close.

In this work, we take a mechanistic approach to explore the opening and closing pathways of the EGJ by looking at how energy is expended at the EGJ during a contraction cycle. To do so, we examine both clinical data and 1D simulations of flow inside a FLIP device. We reveal that there are two possible pressure-cross-sectional area loop patterns at the EGJ and seek to: (i) identify the key characteristics that define each loop type, (ii) find what causes the inversion from one loop to another, and (iii) examine how energy is spent at the EGJ during a single contraction cycle. Doing so helps us identify the mechanisms and physical parameters that characterize EGJ function.

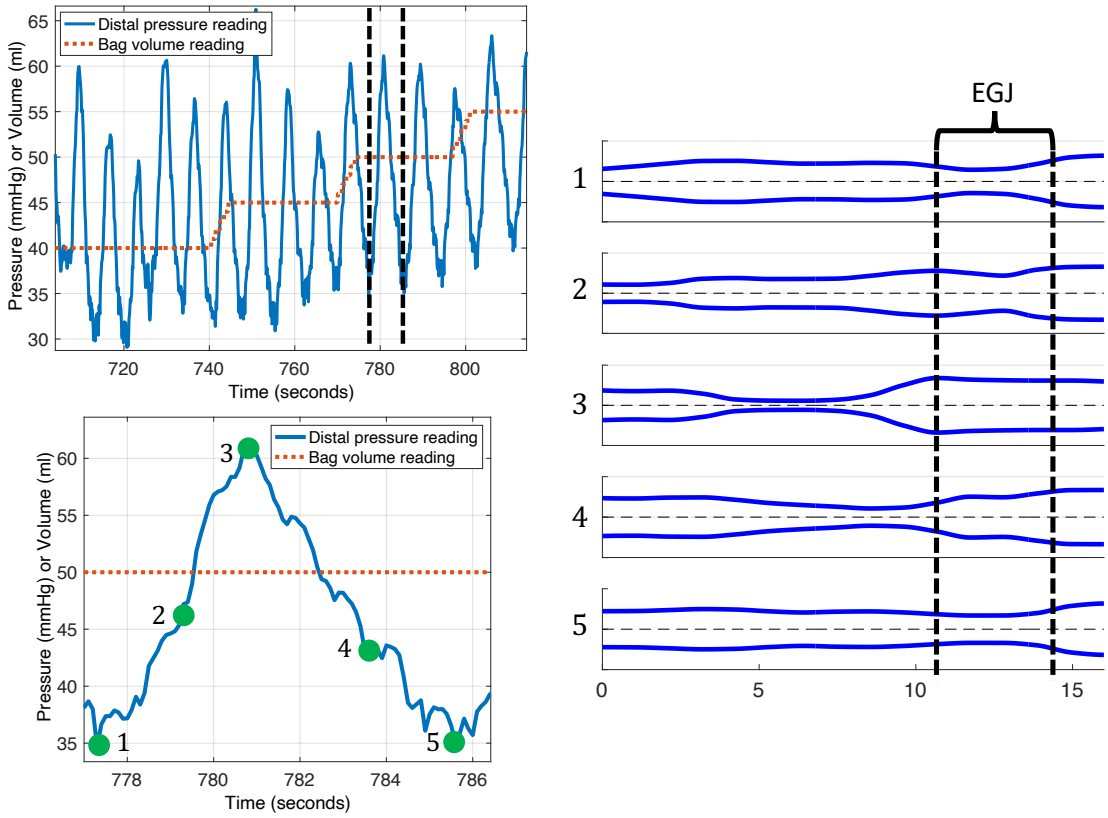

Fig. 1 A visual representation of the clinical data collected from a single subject using a FLIP device. The graph on the top left shows the pressure reading and bag volume as a function of time over 120 seconds duration. The pressure changes as a result of esophageal contractility in response to the distension. The volume increase is dictated by the physician conducting the procedure. The graph on the bottom left is a close-up view of the data between the two dotted lines in the plot above it (between 777.3 seconds and 785.6 seconds). It captures the pressure variation during a single contraction cycle (Carlson et al., 2015). The right figure displays the tube shape at five different time instants, ordered chronologically, corresponding to the five points in the pressure graph, and the location of the EGJ is marked. The pattern in this figure reveal that the increase in pressure at the distal end of the FLIP bag corresponds to the increase of cross-sectional area at the EGJ, and pressure decrease at the end of the contraction cycle corresponds to the decrease of cross-sectional area at the EGJ. The maximum opening of the EGJ occurs at the same time instant as maximum distal pressure.

2 Methods

In this section, we discuss the experimental procedure to collect clinical FLIP data at the EGJ. In addition, we detail the simulation approach taken to reproduce FLIP experiments at different sphincters.

2.1 Subjects

The subject cohort included 24 healthy, asymptomatic adult volunteers. This number excludes subjects with previous diagnosis of esophageal disorders, previous diagnosis of autoimmune, or eating disorders, use of antacids or proton pump inhibitors, body mass index > 30 kg/m^2, or a history of tobacco use or alcohol abuse, as described in Carlson et al. (2021a). The data was collected at the Esophageal Center of Northwestern between November 2012 and October 2018. Informed consent was obtained for subject

participation; who were paid for their participation. The study protocol was approved by the Northwestern University Institutional Review Board. This control cohort overlaps previous publications (Carlson et al., 2021a,b; Acharya et al., 2020; Carlson et al., 2016, 2019; Triggs et al., 2020).

2.2 FLIP Study Protocol

The study was performed during sedated endoscopy using a 16-cm FLIP (EndoFLIP® EF-322N; Medtronic, Inc, Shoreview, MN). The FLIP was inserted transorally, placed in the esophagus lumen, bypassing the LES. The FLIP bag was then filled with saline at 10-mL increments, and the CSA at 16 locations and one distal pressure measurements were recorded as the wall responded to the filling. The bag volume began at 40-mL and increased until reaching 60-mL. Each volume was maintained for 30-60 sec. More information on the experimental procedure is available in Carlson et al. (2021a,b); Acharya et al. (2020); Carlson et al. (2016, 2019).

2.3 Data Analysis

The FLIP data was exported using MATLAB `readtable`. A total of 219 contraction cycles were identified by tracking distal pressure and cross-sectional area at the EGJ. The location of the EGJ was identified as the location with the minimum cross-sectional area at the beginning of the contraction cycle. Due to dry catheter artifact, we omitted 87 data points. Consequently, the study focused on 132 contraction cycles. Dry catheter artifact is when the peristaltic contraction causes occlusion of the FLIP and therefore disrupts the electrical current which is used for the impedance planimetry technology. The pressure at different locations along the FLIP bag can be calculated using the provided distal pressure, as proposed by Halder et al. (2021). Hence, one can plot the pressure-cross-sectional area loops at different locations on the esophagus.

2.4 Simulation of FLIP Experiment

To determine the key parameters that are involved and affect the shape and pattern of the pressure-cross-sectional area hysteresis at the EGJ, we utilize a 1D model. The model attempts to imitate flow inside a FLIP device located in the esophagus by simulating flow inside an elastic tube that is closed on both ends. Our study builds on and extends recent studies by Acharya et al. (2021) and Elisha et al. (2022), who proposed a minimal model for peristaltic flow in a closed-ends flexible tube, and using it to study the esophagus. However, their model did not include the EGJ, which is implemented in this study. Additionally, previous investigations looked at the work done by a peristaltic wave along the entire tube length, without any EGJ contraction. In this work, we focus on the energy expended at the EGJ only by altering the work equations.

2.4.1 Governing Equations in 1D

The mass and momentum conservation equations are

$$\frac{\partial A}{\partial t} + \frac{\partial (Au)}{\partial x} = 0, \tag{1}$$

and

$$\frac{\partial u}{\partial t} + u\frac{\partial u}{\partial x} = -\frac{1}{\rho}\frac{\partial P}{\partial x} - \frac{8\pi\mu u}{\rho A}, \tag{2}$$

respectively. In the equations above, $A(x,t)$, $u(x,t)$, and $P(x,t)$ are the tube cross-sectional area, fluid velocity (averaged at each cross-sectional area), and pressure inside the tube, respectively. The constants ρ and μ are the fluid density and viscosity, respectively. These 1D forms of the continuity and the momentum conservation equations were derived by Ottesen (2003) and have been widely used to describe valveless pumping (Manopoulos et al., 2006; Bringley et al., 2008).

The last equation in this system expresses pressure in terms of the tube's cross-sectional area. This constitutive relation, derived in (Whittaker et al., 2010) and validated experimentally in (Kwiatek et al., 2011) is known as the 'tube law', and takes the form

$$\Delta P = K_e \left(\frac{A(x,t)}{A_o \theta(x,t)} - 1 \right). \tag{3}$$

Here, ΔP is the difference between the pressure inside and outside the tube ($\Delta P = P_i - P_o$), K_e is tube stiffness, and A_o is the undeformed reference area representing the cross-sectional area of the tube when $\Delta P = 0$. Lastly, $\theta(x,t)$ is an activation term which changes the reference cross-sectional area of the tube wall. This term is implemented in order to mimic the function of the esophageal muscle fibers as they contract and relax throughout the contraction cycle (Ottesen, 2003; Manopoulos et al., 2006; Bringley et al., 2008; Mittal, 2016; Abrahao Jr et al., 2011). The activation term $\theta(x,t)$ is expressed as a piecewise function elaborated upon in section 2.4.3.

Since the outside pressure is constant, equation (3) can be written as

$$P(x,t) = K_e \left(\frac{A(x,t)}{A_o \theta(x,t)} - 1 \right) + P_o \tag{4}$$

to solve for the pressure inside the tube. Note that in our simulations, the pressure outside of the tube is assumed to be the reference pressure, so that $P_o = 0$.

2.4.2 Non-dimensionalizing Dynamic Equations

To obtain a better understanding of the physical held of the system and reduce the number of independent variables, we non-dimetionalize equations (1), (2) and (4) using

$$A = \alpha A_o, \qquad t = \tau \frac{L}{c}, \qquad u = Uc, \qquad P = pK_e, \qquad \text{and} \qquad x = \chi L, \tag{5}$$

where α, τ, U, p, and χ are non-dimensional variables of area, time, velocity, pressure, and position, respectively. The terms c and L are dimensional constants for the speed of the peristaltic wave and the length of the tube, respectively.

Therefore, the mass conservation, momentum conservation, and tube law equations can be written as

$$\frac{\partial \alpha}{\partial \tau} + \frac{\partial (\alpha U)}{\partial \chi} = \epsilon \left(\frac{\alpha}{\theta} \right)_{\chi\chi}, \tag{6}$$

$$\frac{\partial U}{\partial \tau} + U \frac{\partial U}{\partial \chi} + \psi \frac{\partial p}{\partial \chi} + \beta \frac{U}{\alpha} = 0, \qquad \text{and} \tag{7}$$

$$p = \left(\frac{\alpha}{\theta} - 1 \right) - f(\alpha, U), \tag{8}$$

respectively. The terms ψ and β are non-dimensional stiffness and viscosity parameters, respectively, defined as $\psi = K_e/(\rho c^2)$ and $\beta = 8\pi\mu L/(\rho A_o c)$. Notice that ψ is inverse of Cauchy number and β is inverse of the Reynolds number. The function $f(\alpha, U)$ is a damping term added to the right hand side of the pressure equation to regularize the system and therefore help stabilize the numerical solution. It is defined as $f(\alpha, U) = \eta \frac{\partial(\alpha U)}{\partial \chi}$ where $\eta = (Y c A_o)/(K_e L)$, and Y is the damping coefficient. An additional discussion is available in (Acharya et al., 2021) and (Wang et al., 2014). Lastly, $\epsilon \left(\alpha/\theta\right)_{\chi\chi}$ is a smoothing term added to the right-hand side of the continuity equation in order to obtain faster convergence and reduce computational time.

Finally, we can plug equation (8) into equation (7) to obtain

$$\frac{\partial U}{\partial \tau} + U \frac{\partial U}{\partial \chi} + \beta \frac{U}{\alpha} + \psi \frac{\partial}{\partial \chi} \left(\frac{\alpha}{\theta} \right) = \zeta \frac{\partial^2}{\partial \chi^2} (\alpha U), \tag{9}$$

such that we have a system of two equations, equations (6), and (9). Here, ζ is equal to the product of η and ψ.

2.4.3 The Peristaltic Wave and Active Relaxation

The activation function $\theta(\chi,\tau)$ multiplies the constant reference area term A_o in the tube law (equation (8)) in order to change the reference area to resemble the activation of the esophageal muscle. We apply this function to the model with the intention of mimicking both the muscle contraction of the traveling wave which pushes fluid forward, as well as the contraction and relaxation of the EGJ muscles. Using an activation function to vary the reference area is often used in instances that the external activation pressure at a specific location varies sinusoidally with time (Acharya et al., 2021; Ottesen, 2003; Manopoulos et al., 2006; Bringley et al., 2008).

In (Acharya et al., 2021; Elisha et al., 2022), the activation function only considered the peristaltic contraction of the traveling wave and wall relaxation, but did not include the EGJ muscle contraction and relaxation. In these studies, the muscle activation was modeled as a sinusoidal wave traveling with time along the length of the elastic tube. The wave had constant amplitude, wave speed, and wavelength. This form of the activation function was supported by clinical data reported in (Goyal and Chaudhury, 2008; Crist et al., 1984). The activation function θ introduced in our model is similar to the ones in (Acharya et al., 2021) and (Elisha et al., 2022), and is defined as a superposition of two piecewise functions, such that

$$\theta(\chi,\tau) = \theta_p(\chi,\tau) + \theta_{\text{EGJ}}(\chi,\tau). \tag{10}$$

Function $\theta_{\text{EGJ}}(\chi,\tau)$ is responsible for the active relaxation of the EGJ and function $\theta_p(\chi,\tau)$ is responsible for the traveling peristalsis as well as the restoration of EGJ tone at the end of the contraction cycle.

The traveling wave activation function $\theta_p(\chi,\tau)$ takes the form

$$\theta_p(\chi,\tau) = \begin{cases} 1 - \frac{1-\theta_c}{2}\left[1 + \sin\left(\frac{2\pi}{\text{w}}\left(\chi-\tau\right) + \frac{3\pi}{2}\right)\right], & \tau - \text{w} \le \chi \le \tau,\ \tau \le \chi_2 \\ 1 - \frac{1-\theta_c}{2}\left[1 + \sin\left(\frac{2\pi}{\text{w}}\left(\chi-\chi_2\right) + \frac{3\pi}{2}\right)\right], & \chi_1 \le \chi \le \chi_2,\ \tau > \chi_2 \\ 1, & \text{otherwise.} \end{cases} \tag{11}$$

In the equation above, θ_c is the peristaltic contraction strength, w is the non-dimensional width of the peristaltic wave, and χ_1 and χ_2 are the boundaries of the EGJ segment, where $\chi_2 > \chi_1$ and the width of the EGJ is $\text{w}_{\text{EGJ}} = \chi_2 - \chi_1$. In this work, $\text{w}_{\text{EGJ}} = \text{w}$. Function θ_p is plotted at two time instance, τ_1 and τ_2 in figures 2a and 2b, respectively, where $\tau_1 < \chi_2$ and $\tau_2 > \chi_2$. As the figures show, while $\tau \le \chi_2$, the wave defined by $\theta_p(\chi,\tau)$ travels with time along the length of the domain. Once $\tau > \chi_2$, the wave stops traveling in time yet conserves its form (figure 2b).

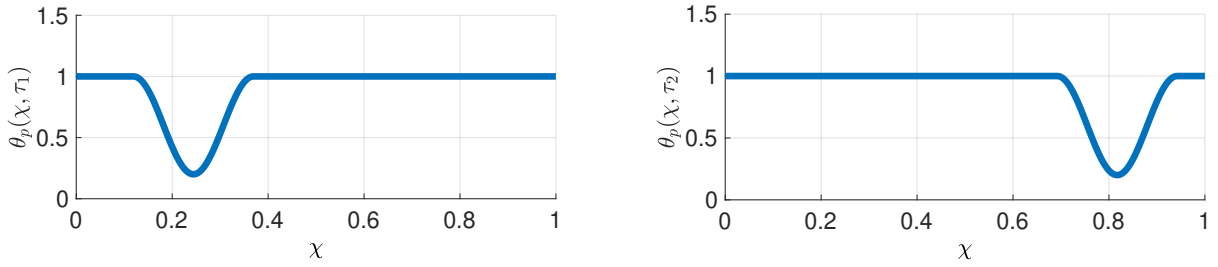

(a) $\tau = \tau_1 < \chi_2$ **(b)** $\tau = \tau_2 > \chi_2$

Fig. 2 Two plots of function $\theta_p(\chi,\tau)$ defined in equation (11), at (a) $\tau = \tau_1 < \chi_2$ and (b) $\tau = \tau_2 > \chi_2$.

Function $\theta_{\text{EGJ}}(\chi,\tau)$ is a piecewise function which mimics the initial contraction and active relaxation of EGJ tone. Different than function θ_p, function θ_{EGJ} does not travel with time, but its amplitude decreases with time. The function is defined such that

$$\theta_{\text{EGJ}}(\chi,\tau) = \begin{cases} \frac{\theta_r\theta_R(\tau)-1}{2}\left[1 + \sin\left(\frac{2\pi}{\text{w}_{\text{EGJ}}}\left(\chi-\chi_2\right) + \frac{3\pi}{2}\right)\right], & \chi_1 \le \chi \le \chi_2 \\ 0, & \text{otherwise.} \end{cases} \tag{12}$$

where θ_r is the EGJ contraction strength and

$$\theta_R(\tau) = \begin{cases} 1, & \tau \leq \tau_i \\ 1 + \frac{1+\frac{1}{\theta_r}}{\tau_m - \tau_i}(\tau - \tau_i), & \tau_i < \tau \leq \tau_m \\ \frac{1}{\theta_r}, & \tau_m < \tau. \end{cases} \tag{13}$$

In the equation above, τ_i marks the time instance at which the EGJ wall starts relaxing, and τ_m marks the time instance at which the EGJ wall is fully relaxed. We define the relaxation time as $\gamma = \tau_m - \tau_i$.

As equations (12) and (13) indicate, at the beginning of the the contraction cycle ($0 \leq \tau < \tau_i$), the EGJ is contracted, and therefore the shape of $\theta_{\text{EGJ}}(\chi, \tau = 0)$ is similar to θ_p when $\tau > \chi_2$ (figure 2b). Once $\tau = \tau_i$, the EGJ wall starts relaxing, until $\tau = \tau_m$. At $\tau > \tau_m$, the EGJ is fully relaxed. Note that the active contraction of the EGJ at the end of the contraction cycle is obtained by the peristaltic contraction wave function θ_p traveling down the length of the tube and stopping at the EGJ location (stops at $\chi_1 \leq \chi \leq \chi_2$, $\tau > \chi_2$). For this to occur, we set θ_r=θ_c.

The value of γ dictates the EGJ relaxation speed, which introduces a new physical component into the parameters that define the problem. Small γ implies fast relaxation of the EGJ wall and large γ implies slow relaxation of the EGJ wall. Figure 3 presents tube deformations of two simulations at five different time instants. Figure 3a displays a case with slow relaxation of the EGJ wall while figure 3b displays a case with fast relaxation of the EGJ wall, such that $\gamma_a > \gamma_b$. As the two figures show, at the first time instant, the EGJ walls of both tubes are equally contracted. However, at the second time instant, this is no longer the case. While the contraction strength of the EGJ of tube (a) has barely changed from the previous time instant, the EGJ at case (b) is almost fully relaxed. Note that both cases start relaxing at the same time and relax to the same maximum relaxation. However, case (b) reaches full relaxation earlier in the cycle when compared to case (a).

Figure 4 presents a plot of the activation function θ at time instant τ_1. The figure shows how functions θ_p and θ_{EGJ} apply simultaneously to the tube wall. While the peristaltic contraction wave travels down the length of the tube at constant contraction (θ_c) and speed (c), the tone at the EGJ relaxes.

2.4.4 Boundary and Initial Conditions

The elastic tube is closed on both ends and the volume inside the tube remains constant such that there is no flow in or out of the tube. Therefore

$$U(\chi = 0, \tau) = 0 \qquad \text{and} \qquad U(\chi = 1, \tau) = 0. \tag{14}$$

The boundary condition for α is obtained by applying the velocity boundary condition in equation (14) into equation (7), which implies that $\partial p/\partial \chi = 0$. Therefore, by taking the spatial derivative of equation (8) and setting it equal to zero, we obtain a Neumann boundary condition for α (the non-dimensional cross-sectional area) of the form,

$$\frac{\partial}{\partial \chi}\left(\frac{\alpha}{\theta}\right)\bigg|_{\chi=0,\tau} = 0 \qquad \text{and} \qquad \frac{\partial}{\partial \chi}\left(\frac{\alpha}{\theta}\right)\bigg|_{\chi=1,\tau} = 0. \tag{15}$$

Note that this condition is derived assuming that $\eta \approx 0$. However, as explained in (Acharya et al., 2021), the effects due to this damping at the boundary are negligible even when η is small but not equal to zero.

At $\tau = 0$, the traveling peristaltic wave has yet to enter the domain and the EGJ is contracted, therefore, the fluid velocity inside the tube is equal to zero everywhere. The cross-sectional area at $\tau = 0$ depends on the volume of the fluid filling the tube. In this resting state the pressure in the tube would be uniform (typically positive), which according to the tube law implies that α/θ is a constant ($= S_{\text{IC}}$) for the initially filled tube. Hence, the initial conditions are specified as such:

$$U(\chi, \tau = 0) = 0 \qquad \alpha(\chi, \tau = 0) = S_{\text{IC}}\theta(\chi, \tau = 0). \tag{16}$$

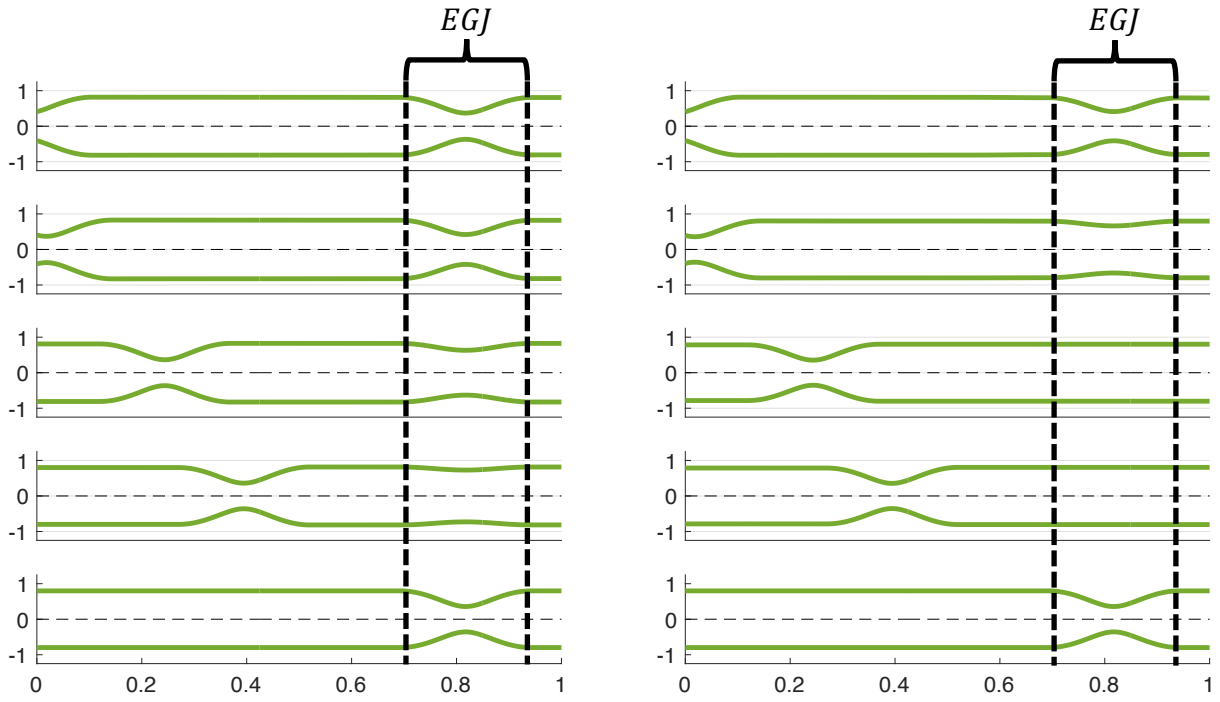

(a) Slow EGJ wall relaxation

(b) Fast EGJ wall relaxation

Fig. 3 Tube deformation of two simulations. (a) EGJ contraction relaxes slowly in relation to the peristaltic contraction wave entering the domain. (b) EGJ contraction relaxes rapidly in relation to the peristaltic contraction wave entering the domain. Both examples start relaxing at the same time but reach (the same) maximum relaxation at different times.

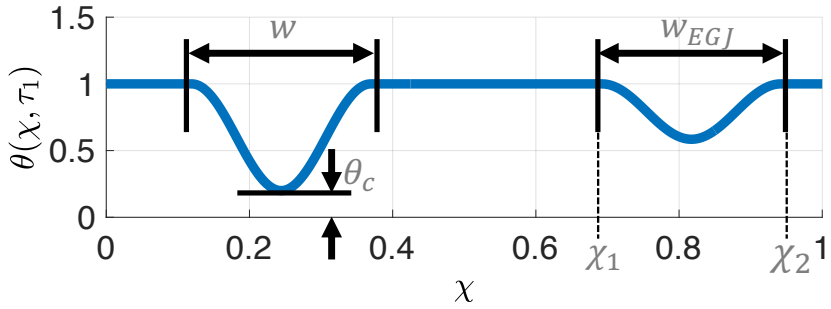

Fig. 4 A plot of the activation function θ from equation (10) along the tube length at a single time instant τ_1.

2.4.5 Numerical Implementation

The MATLAB `pdepe` function is used to obtain the numerical solution of $\alpha(\chi, \tau)$ and $U(\chi, \tau)$ by solving equations (6) and (9) with the boundary and initial conditions in equations (14), (15), and (16), respectively. The simulations are differentiated by a unique combination of the physical parameters defining this problem, listed in table 1. Changing the parameters ψ, β, θ_c, and γ corresponds to examining the effect of tube wall stiffness, wave speed, contraction strength, fluid density, fluid viscosity and EGJ relaxation speed on the

tube deformation (Acharya et al., 2021). The computational procedure to solve this forward simulation is described in greater details by Acharya et al. (2021), who also validates the 1D model by comparing it to an equivalent 3D immersed boundary simulation.

The values for the parameters listed in table 1 are prescribed as follows. The values for w and $\mathrm{w_{EGJ}}$ are determined by scaling a typical value of the width of the traveling contraction and the EGJ by the FLIP length. The values for θ_c and θ_r are assigned based on the results in (Halder et al., 2021) and (Elisha et al., 2022), which showed that θ_c is of order 10^{-1}. The values for γ are estimated by scaling the time it takes the EGJ to open by the time it takes to complete a typical contraction cycle. The value for S_{IC} depends on the constant volume of the bag, such that $S_{\mathrm{IC}} = V/(A_o \int_0^L \theta_{\mathrm{IC}}(x)dx)$, where V is bag volume. This value can go up to 4. Lastly, ψ and β span over a large range to cover all possible phenomena. Small β (order 1) and large ψ (order 10^3) correspond to typical clinical values. However, this range only captures scenarios wherein viscous effects are negligible. Therefore, we also include high β and small ψ values. Note that there is no difference in the results for $\beta = 1$ or 100, hence $\beta = 100$ represents experimental case.

Table 1: List of non-dimensional parameters

Symbol	Values	Definition
β	$100 - 10,000$	Dimensionless strength of viscous effects (inverse of Reynolds number)
ψ	$100 - 10,000$	Dimensionless rigidity of the elastic tube (inverse of Cauchy number)
γ	$0.06 - 0.6$	Dimensionless EGJ relaxation speed
θ_c	$0.05 - 0.2$	Peristaltic contraction strength
θ_r	$0.05 - 0.2$	EGJ contraction strength
w	0.25	Width of peristaltic wave
$\mathrm{w_{EGJ}}$	0.25	EGJ width
S_{IC}	$1.25 - 2.0$	Constant area that depends on the volume of the bag ($\alpha(\tau = 0)/\theta(\tau = 0)$)

2.5 Work Balance

In this section, we will derive an equation to examine the way in which energy is expended during a contraction cycle. This will helps us reveal the leading parameters that control the hysteresis.

To derive the work balance equation, we multiply the momentum equation (2) by the flow rate $Q = Au$, and rewrite it such that

$$A\frac{\partial}{\partial t}\left(\frac{1}{2}\rho u^2\right) + Q\frac{\partial}{\partial x}\left(\frac{1}{2}\rho u^2\right) = -Au\frac{\partial P}{\partial x} - \frac{8\pi\mu u Q}{A}. \tag{17}$$

Next, we add the continuity equation to the left hand side of equation (17) and rearrange it to obtain

$$\frac{\partial}{\partial t}\left(\frac{1}{2}\rho A u^2\right) + \frac{\partial}{\partial x}\left(\frac{1}{2}\rho Q u^2\right) = -\frac{\partial\left(AuP\right)}{\partial x} + P\frac{\partial\left(Au\right)}{\partial x} - \frac{8\pi\mu u Q}{A}. \tag{18}$$

From equation (1), we can replace $\partial\left(Au\right)/\partial x$ with $-\partial A/\partial t$, to acquire the final form of the momentum equation

$$\frac{\partial}{\partial t}\left(\frac{1}{2}\rho A u^2\right) + \frac{\partial}{\partial x}\left(\frac{1}{2}\rho Q u^2\right) = -\frac{\partial\left(AuP\right)}{\partial x} - P\frac{\partial A}{\partial t} - \frac{8\pi\mu u Q}{A}. \tag{19}$$

Integrating equation (19) with respect to length results in a power conservation equation of the form

$$\underbrace{-\int_{x_1}^{x_2} P\frac{\partial A}{\partial t}\mathrm{d}x}_{\mathrm{I}} = \underbrace{\frac{\partial}{\partial t}\int_{x_1}^{x_2}\left(\frac{1}{2}\rho A u^2\right)\mathrm{d}x}_{\mathrm{II}} + \underbrace{\int_{x_1}^{x_2} 8\pi\mu u^2\mathrm{d}x}_{\mathrm{III}} + \underbrace{\left(AuP\right)\Big|_{x_1}^{x_2}}_{\mathrm{IV}} + \underbrace{\left(\frac{1}{2}\rho A u^3\right)\Big|_{x_1}^{x_2}}_{\mathrm{V}}. \tag{20}$$

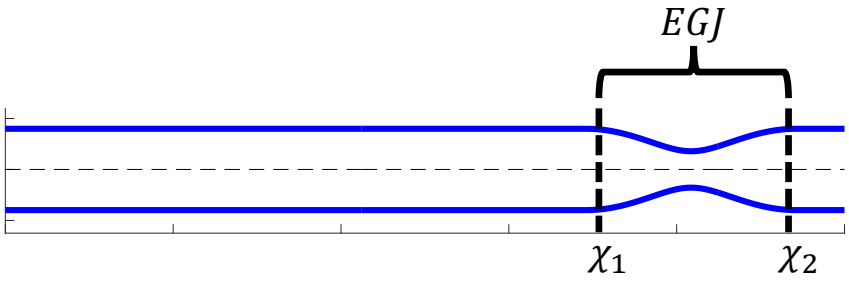

Fig. 5 Image showing the EGJ location on the elastic tube at $\tau = 0$.

The equation above is the power balance equation. The left hand side is the rate of work done by the tube wall, and the right hand side includes different ways in which the power is 'consumed' in the section of the esophagus between x_1 and x_2 (called the 'test section'). Each term in equation (20) is numbered, where (I) is the rate of work done by the tube wall on the fluid within the test section, (II) is the rate of change in kinetic energy of the fluid within the test section, (III) is the rate of energy loss due to viscous dissipation in the test section, (IV) is the net rate of work done by the fluid within the test section on the fluid adjacent to the test section by way of pressure acting on the cross-sections of either ends of the test section (for reference: this is the negative of the power due to the driving pressure gradient in pipe flows), and (V) is the net flux of kinetic energy out of the test section.

Integrating equation (20) with respect to time results in the work balance equation, such that

$$\begin{aligned} -\int_{t_1}^{t_2}\int_{x_1}^{x_2} P\frac{\partial A}{\partial t}\mathrm{d}x\mathrm{d}t = \int_{t_1}^{t_2}\frac{\partial}{\partial t}\int_{x_1}^{x_2}\left(\frac{1}{2}\rho A u^2\right)\mathrm{d}x\mathrm{d}t + \int_{t_1}^{t_2}\int_{x_1}^{x_2} 8\pi\mu u^2 \mathrm{d}x\mathrm{d}t \\ + \int_{t_1}^{t_2}(AuP)\Big|_{x_1}^{x_2}\mathrm{d}t + \int_{t_1}^{t_2}\left(\frac{1}{2}\rho A u^3\right)\Big|_{x_1}^{x_2}\mathrm{d}t. \end{aligned} \tag{21}$$

The non-dimensional form of equation (21) is

$$\begin{aligned} -\psi\int_{\tau_1}^{\tau_2}\int_{\chi_1}^{\chi_2} p\frac{\partial \alpha}{\partial \tau}\mathrm{d}\chi\mathrm{d}\tau = \int_{\tau_1}^{\tau_2}\frac{\partial}{\partial \tau}\int_{\chi_1}^{\chi_2}\left(\frac{1}{2}\alpha U^2\right)\mathrm{d}\chi\mathrm{d}\tau + \beta\int_{\tau_1}^{\tau_2}\int_{\chi_1}^{\chi_2} U^2\mathrm{d}\chi\mathrm{d}\tau \\ + \psi\int_{\tau_1}^{\tau_2}(\alpha U p)\Big|_{\chi_1}^{\chi_2}\mathrm{d}\tau + \int_{\tau_1}^{\tau_2}\left(\frac{1}{2}\alpha U^3\right)\Big|_{\chi_1}^{\chi_2}\mathrm{d}\tau. \end{aligned} \tag{22}$$

In our case, we want to look at the work balance throughout the entire contraction cycle, and therefore, $\tau_1 = 0$ and $\tau_2 = \tau_f$ where τ_f is the final, non-dimensional time instant. For work balance along the entire esophageal length, we set $\chi_1 = 0$ and $\chi_2 = 1$. For work balance at the EGJ, we specify the 'EGJ region' of width $\mathrm{w_{EGJ}} = \chi_2 - \chi_1 = 0.25$ (seen in figure 5), where $\chi_1 = 0.70$ and $\chi_2 = 0.95$.

2.5.1 Passive & Active Work Decomposition

First we will define active and passive pressure and then we will define active and passive work. The pressure term can be considered to have contributions from both the passive expansion of the tube wall and the pressure rise or drop due to active contraction or relaxation of the wall (Acharya et al., 2021). Correspondingly, the total work done by the tube wall on the fluid (LHS of equation (21)) will be the sum of the passive and active work. Decomposing the total work into its active and passive components makes it convenient to explain the difference between the two pressure-area loop types, as discussed in section 3.

We decompose the total pressure into its active and passive components:

$$P(x,t) = P_{\text{passive}} + P_{\text{active}}. \tag{23}$$

Consider a tube in its unstressed (zero pressure) configuration with $\theta_{\text{IC}}(x) = \theta(x, t = 0)$ as the activation function. Now imagine deforming this tube to any instantaneous configuration $A(x,t)$ without changing the activation function $\theta_{\text{IC}}(x)$. The equilibrium pressure (the pressure needed to balance the elastic stress) inside the tube in this *passively* deformed state is defined as the passive pressure

$$P_{\text{passive}}(x,t) = K_e \left(\frac{A(x,t)}{A_o \theta_{\text{IC}}(x)} - 1 \right), \tag{24}$$

where $P_o = 0$ has been used. The non-dimensional form of equation (24) is

$$p_{\text{passive}}(\chi,\tau) = \frac{\alpha(\chi,\tau)}{\theta_{\text{IC}}(\chi)} - 1. \tag{25}$$

Now imagine that the deformed configuration in the above thought experiment is held fixed at $A(x,t)$ while the activation function is changed from $\theta_{\text{IC}}(x)$ to the actual instantaneous activation function $\theta(x,t)$. Since the reference state of the tube is changed actively, the equilibrium pressure required to balance the elastic stress would change. This change in equilibrium pressure caused by the change in the activation function is defined as the active pressure

$$P_{\text{active}}(x,t) = K_e \frac{A(x,t)}{A_o} \left(\frac{1}{\theta(x,t)} - \frac{1}{\theta_{\text{IC}}(x)} \right) \tag{26}$$

and the non-dimensional form of the active pressure is

$$p_{\text{active}}(\chi,\tau) = \alpha \left(\frac{1}{\theta(\chi,\tau)} - \frac{1}{\theta_{\text{IC}}(\chi)} \right). \tag{27}$$

Using the above decomposition of pressure, equation (21) can be written as

$$\begin{aligned} -\int_{t_1}^{t_2}\int_{x_1}^{x_2} P_{\text{active}} \frac{\partial A}{\partial t} \mathrm{d}x\mathrm{d}t = \int_{t_1}^{t_2} \frac{\partial}{\partial t} \int_{x_1}^{x_2} \left(\frac{1}{2}\rho A u^2 \right) \mathrm{d}x\mathrm{d}t + \int_{t_1}^{t_2}\int_{x_1}^{x_2} 8\pi\mu u^2 \mathrm{d}x\mathrm{d}t \\ + \int_{t_1}^{t_2} (AuP)\Big|_{x_1}^{x_2} \mathrm{d}t + \int_{t_1}^{t_2} \left(\frac{1}{2}\rho A u^3 \right)\Big|_{x_1}^{x_2} \mathrm{d}t + \int_{t_1}^{t_2}\int_{x_1}^{x_2} P_{\text{passive}} \frac{\partial A}{\partial t} \mathrm{d}x\mathrm{d}t, \end{aligned} \tag{28}$$

and equation (22) becomes

$$\begin{aligned} -\psi \int_{\tau_1}^{\tau_2}\int_{\chi_1}^{\chi_2} p_{\text{active}} \frac{\partial \alpha}{\partial \tau} \mathrm{d}\chi\mathrm{d}\tau = \int_{\tau_1}^{\tau_2} \frac{\partial}{\partial \tau} \int_{\chi_1}^{\chi_2} \left(\frac{1}{2}\alpha U^2 \right) \mathrm{d}\chi\mathrm{d}\tau + \beta \int_{\tau_1}^{\tau_2}\int_{\chi_1}^{\chi_2} U^2 \mathrm{d}\chi\mathrm{d}\tau \\ + \psi \int_{\tau_1}^{\tau_2} (\alpha U p)\Big|_{\chi_1}^{\chi_2} \mathrm{d}\tau + \int_{\tau_1}^{\tau_2} \left(\frac{1}{2}\alpha U^3 \right)\Big|_{\chi_1}^{\chi_2} \mathrm{d}\tau + \psi \int_{\tau_1}^{\tau_2}\int_{\chi_1}^{\chi_2} p_{\text{passive}} \frac{\partial \alpha}{\partial \tau} \mathrm{d}\chi\mathrm{d}\tau, \end{aligned} \tag{29}$$

which is the non-dimensional form of equation (28). The term involving active pressure is defined as the active work, whereas the term involving passive pressure is defined as the passive work (also to be referred to as the passive elastic energy).

Notice that the passive pressure term is moved to the RHS of the equation. In this form of the equation, the work done by the active pressure is equal to the consumers of this active work, which includes the passive elastic energy of the tube wall (the passive pressure term on the RHS). We emphasize that the passive elastic

energy of the wall is not the actual elastic energy stored in the wall for a given configuration. It is the energy that would have been stored in the wall if the tube were deformed to its current configuration $A(x,t)$ without changing the activation function from the initial state $\theta_{\text{IC}}(x)$ to its current state $\theta(x,t)$.

Note that the proposed definitions of the passive and active pressures in equations (25) and (27), respectively, ensure that two important consistency conditions are satisfied. First, note that at $\tau = 0$, the traveling peristaltic wave has yet to enter the domain and the EGJ is contracted, therefore the active pressure must be equal to zero for all χ. To verify that, recall that $\theta = \theta_{\text{IC}}$ at $\tau = 0$. Plugging this into equation (27) yields $p_{\text{active}} = 0$ for all χ. Second, at $\tau = 0$, the total pressure ($p = p_{\text{active}} + p_{\text{passive}}$) must be uniform along the tube. Since $p_{\text{active}} = 0$ initially, it implies that p_{passive} should be uniform along the tube at the initial instant. Recall the initial condition that $\alpha(\chi, \tau = 0) = S_{\text{IC}}\theta_{\text{IC}}(\chi)$, where S_{IC} is a constant. Using equation (25), $p_{\text{passive}} = S_{\text{IC}} - 1$, which is a constant for all χ.

3 Results and Discussion

3.1 Clinical Pressure-Area Loops at the EGJ

Figure 6 presents two plots of the pressure at the EGJ as a function of EGJ cross-sectional area during contraction cycles in two different subjects. The pressure-area plot creates a loop with distinct opening and closing curves (marked in blue and red, respectively), which indicates that there is some energy that is being gained or lost by the EGJ. By making the distinction between the opening and closing curves, we identified two physically distinct loop types. The first loop type, displayed in figure 6a looks like a typical hysteresis loop, wherein the opening curve is above the closing curve. In contraction cycles with this loop type, the dominant source of energy in the opening and closing cycle of the EGJ is the contraction wave. This loop type will be called the pressure dominant loop (PDL) and it appears in 34% of the contraction cycles. The second loop type, displayed in figure 6b is flipped, where the closing curve is above the opening curve. In contraction cycles with this loop type, the dominant source of energy in the opening and closing cycle of the EGJ is the active relaxation and contraction of the EGJ tone. This loop type will be called the tone dominant loop (TDL) and it appears in 55% of the contraction cycles. The reason behind these names is in the succeeding section. Note that the remaining 11% are contraction cycles in which a clearly defined loop is not obtained (the opening and closing curves cross one another).

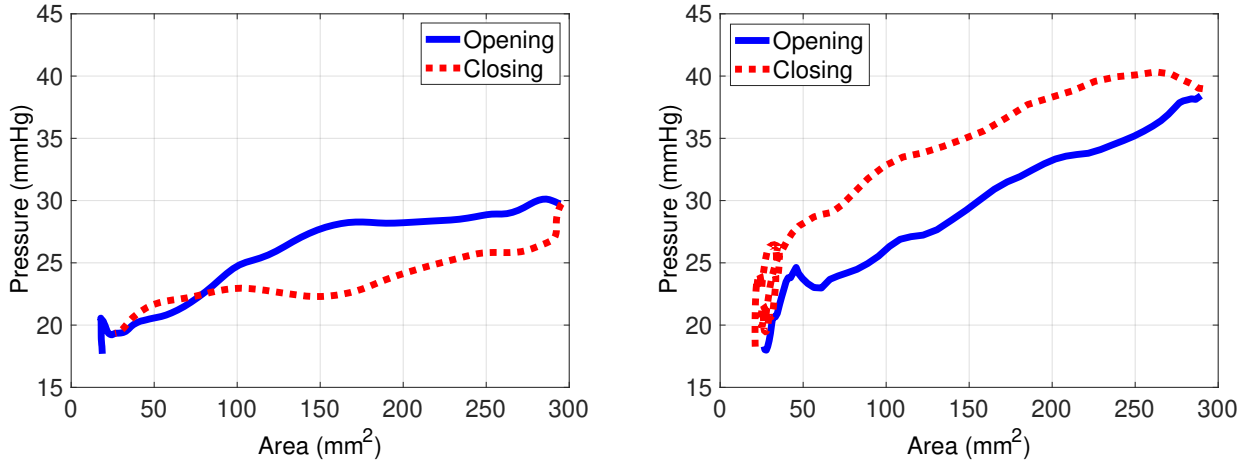

(a) Pressure dominant loop

(b) Tone dominant loop

Fig. 6 Two plots of the pressure-cross-sectional area at the esophagogastric junction extracted from two different contraction cycles of two different subjects recorded clinically by a FLIP device. The plots show two different loop types that arise in clinical data at the esophagogastric junction.

3.2 Simulation Pressure-Area Loops at the EGJ

In the rest of this section, we use our simulation results to identify the key characteristics that define each loop type the physical parameters that cause one loop to occur rather than the other. This is done by considering the energy balance in the tube over time. In the first part of this section, we analyze the simulation results over the entire tube length so that the overall energy balance is clear to the reader but subsequently our main efforts focus on the EGJ. Later, we utilize the conclusions obtained by the simulation results and apply them to clinical data. As discussed later in this section, the key parameters that affect the loop types are ψ, β, and γ. Hence, all simulation results presented in this section use the same values for θ_c, θ_r, w, $\mathrm{w}_{\mathrm{EGJ}}$, and S_{IC}, which are 0.2, 0.2, 0.25, 0.25, and 2, respectively.

3.2.1 Work Curves for the Entire Tube Length

We first look at the work balance over time along the entire esophageal length. Since the tube is closed on both ends, the velocity at both ends is zero, and equation (29) simplifies to

$$-\psi \int_{\tau_1}^{\tau_2}\int_{\chi_1}^{\chi_2} p_{\mathrm{active}} \frac{\partial \alpha}{\partial \tau} \mathrm{d}\chi \mathrm{d}\tau = \int_{\tau_1}^{\tau_2} \frac{\partial}{\partial \tau} \int_{\chi_1}^{\chi_2} \left(\frac{1}{2}\alpha U^2\right) \mathrm{d}\chi \mathrm{d}\tau + \beta \int_{\tau_1}^{\tau_2}\int_{\chi_1}^{\chi_2} U^2 \mathrm{d}\chi \mathrm{d}\tau + \psi \int_{\tau_1}^{\tau_2}\int_{\chi_1}^{\chi_2} p_{\mathrm{passive}} \frac{\partial \alpha}{\partial \tau} \mathrm{d}\chi \mathrm{d}\tau. \tag{30}$$

Figure 7 presents a plot of the work components in equation (30), normalized by ψ ($w = \mathrm{Work}/\psi$), as a function of time. The data plotted in the figure are extracted from one simulation of a single contraction cycle, and the spatial integration is over the entire tube length. In this simulation, $\beta = 100$, $\psi = 100$, and $\gamma = 0.6$. Note that the values of β and ψ considered in this analysis are much greater than 1. The kinetic energy term (first term on the right hand side of equation (30)) is very small compared to the other terms and thus not plotted.

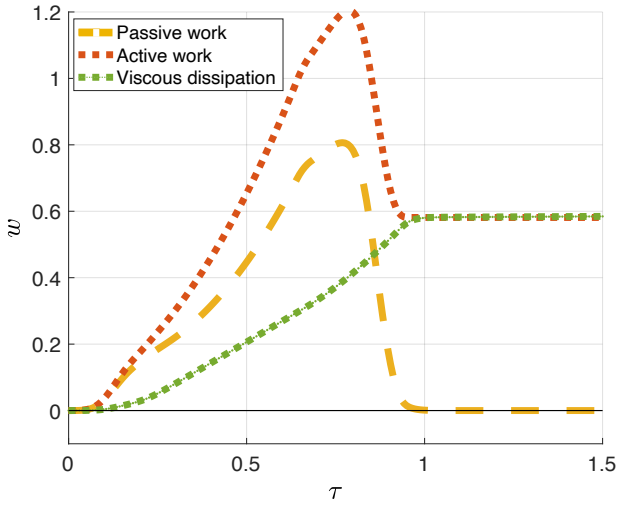

Fig. 7 Passive, active, and viscous work curves along the entire esophageal length as a function of time. At each time instant, the sum of the energy loss due to viscous dissipation and the passive energy stored in the tube wall is equal to the active work done by the tube wall on the fluid. Each curve depicts the cumulative work done in the corresponding mode up to a given time instant.

Figure 7 shows that at $\tau = 0$, immediately prior to the peristaltic wave traveling into the domain; all work components are equal to zero. However, once the contraction wave begins traveling and the EGJ begins relaxing ($\tau \approx 0.1$), all three components start increasing, each having a unique pattern. Note that each curve depicts the cumulative work done in the corresponding mode up to a given time instant.

The passive elastic energy of the tube wall (last term on the right hand side of equation (30)) increases as a result of the expansion of the tube wall. This increase continues until $\tau \approx 0.70$, when the peristaltic wave begins contracting the EGJ, making the tube cross-sectional area closer to its original shape. Hence the passive energy starts decreasing. The sharp decrease continues until the end of the contraction cycle, when the passive energy recovers ($w_{\text{passive,final}} = 0$), indicating that the tube returned to its original shape.

The active work done by the wall on the fluid (the left hand side of equation (30)) curve has a similar pattern. It increases with time as a result of both the contraction wave and EGJ relaxation. Once $\tau \approx 0.70$, the active work that is defined by the change in θ starts decreasing since the contraction of the EGJ brings θ closer to θ_{IC}. Lastly, the curve showing the energy loss due to viscous dissipation (second term on the right hand side of equation (30)) has a different pattern. It maintains a steady increase throughout the contraction cycle, which ends when the peristaltic wave stops traveling. Since viscous dissipation cannot be recovered, $w_{\text{viscous}} \neq 0$ at the end of the cycle. Hence, the active work at the end of the cycle is equal to the energy that is dissipated. All the active work, coming either from contraction in the body of the esophagus or from the relaxation within the EGJ region, is eventually lost via viscous dissipation.

3.2.2 Work Curves for the EGJ Region

In this section, we focus on a portion of the tube length, which we referred to as 'EGJ region.' Note that in this case there are a few additional terms that arise in the work balance compared to the entire tube case. We determine the total work done by the EGJ wall on the fluid over time and examine how this work relates to the pressure-area loop and the shape of the tube. Moreover, we look at the work balance at the EGJ region over time by plotting the curves of each of the work components from equation (29) as a function of time. The limits of the spatial integration in this case were discussed in section 2.5.

Figure 8 presents the results of a typical single contraction cycle simulation with $\beta = 100$, $\psi = 100$, and $\gamma = 0.6$. The graph at the top left displays the total work done by the EGJ wall on the fluid as a function of time. This is calculated using the total pressure instead of just active or passive pressure components. The bottom left figure presents the corresponding pressure-area loop at the EGJ location. The five points highlighted on the loop and the work curve represent five time instants in the contraction cycle. The tube profiles at these five instants are plotted on the right. Highlighting these instants allows us to relate the total work done by the EGJ wall on the fluid to the pressure-area loop, which helps us to better understand the loop types.

$\boldsymbol{\tau \leq \tau_1}$. Initially, right before the peristaltic contraction enters the domain, the EGJ is contracted and the total work done by the EGJ wall on the fluid is equal to zero.

$\boldsymbol{\tau_1 < \tau < \tau_3}$. Between τ_1 and τ_3, the peristaltic contraction wave travels along the length of the tube and, simultaneously, the EGJ actively relaxes. Together, they cause an increase in the cross-sectional area and the pressure at the EGJ, as seen in the loop in figure 8. Since the EGJ opens, it does negative work on the fluid, which explains why the work in the top left of figure 8 is negative between τ_1 and τ_3. The total work done by the EGJ wall during opening is therefore $w_{\text{open}} = -\psi \int_{\tau_1}^{\tau_3} \int_{\chi_1}^{\chi_2} p \frac{\partial \alpha}{\partial \tau} \mathrm{d}\chi \mathrm{d}\tau$, represented by the solid blue arrow in figure 9.

$\boldsymbol{\tau = \tau_3}$. At this instant, the EGJ is fully open, corresponding to the minimum point on the work plot in figure 8.

$\boldsymbol{\tau_3 < \tau < \tau_5}$. Between τ_3 and τ_5, the peristaltic wave travels into the EGJ region which eventually closes the EGJ. In this process, the cross-sectional area and pressure at the EGJ generally decrease as seen in the loop in figure 8. Since the EGJ wall closes, it squeezes the fluid, applying positive work, which is seen on the work plot in figure 8 by an increase in work between points 3 and 5. The total work done by the EGJ wall during closing is therefore $w_{\text{close}} = -\psi \int_{\tau_3}^{\tau_5} \int_{\chi_1}^{\chi_2} p \frac{\partial \alpha}{\partial \tau} \mathrm{d}\chi \mathrm{d}\tau$, represented by the dotted red arrow in figure 9.

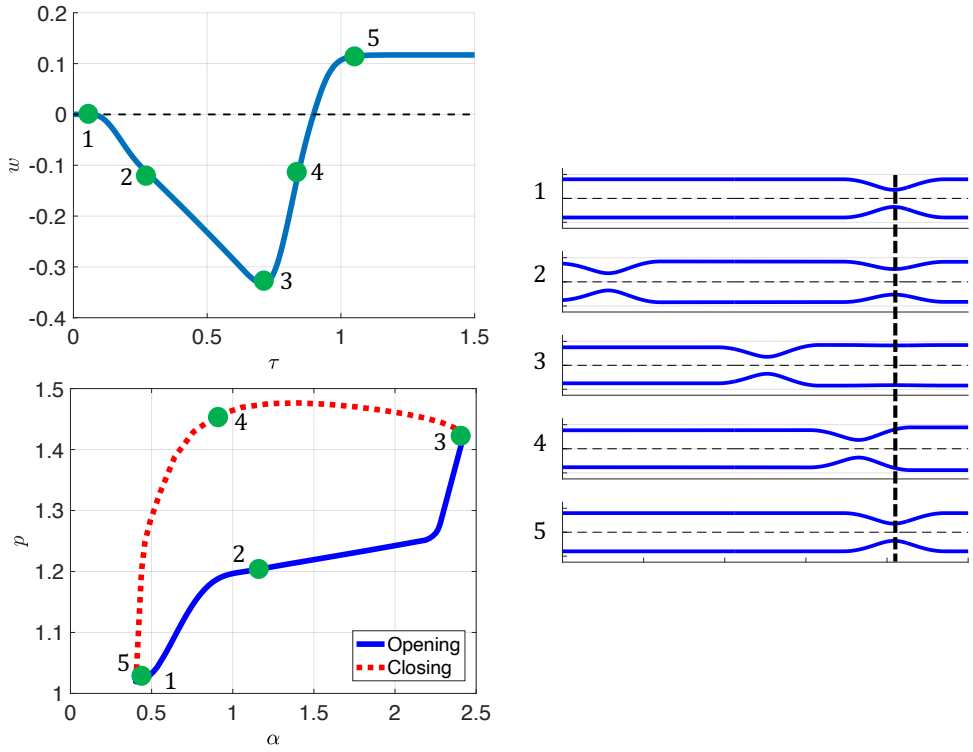

Fig. 8 Simulation results of a single contraction cycle. The graph at the top left shows the curve of the cumulative total work done by the EGJ wall on the fluid as a function of time. The plot at the bottom left presents the corresponding pressure-area loop as recorded at the EGJ location. The right figure displays the tube profile at five consecutive instants, ordered chronologically, corresponding to the five points highlighted on the two left plots.

$\boldsymbol{\tau \geq \tau_5}$**.** Finally, the peristaltic wave stops traveling and the tube returns to its initial shape. The final work value is equal to the work done by the EGJ wall on the fluid during the entire cycle.

The work done by the EGJ wall through the entire contraction cycle is equal to the difference in the magnitude of the work needed to close the EGJ to the work needed to open the EGJ. In figure 9, it is the difference between the length of the dotted red and solid blue arrows. If the final value is positive, as it is in figures 8 and 9, more work is needed to close the EGJ than to open it. On the other hand, if the work value at the end of the cycle is negative, more work is needed to open the EGJ than to close it.

Before we proceed to understand how this relates to the two loop types identified earlier (figures 6a and 6b), we will consider the detailed work balance in the EGJ region. Figure 10 presents the work components from equation (29) evaluated at the EGJ region as a function of time. The rate of change of kinetic energy and the kinetic energy flux terms are not plotted in the figure since $\psi >> 1$ and $\beta >> 1$ and consequently these contributions are small.

As figure 10 shows, the active (left hand side of equation (29)), passive (last term on the right hand side of equation (29)), and viscous dissipation (second term on the right hand side of equation (29)) terms display similar trends to the ones described in section 3.2.1 with one additional observation. The total viscous dissipation in the EGJ region at the end of the contraction cycle is not equal to that the active work done by the EGJ wall on the fluid. There is an additional contribution. Notice how the active work and viscous dissipation curves are not superimposed on one another at the end of the cycle in figure 10. The final viscous dissipation is greater than the total active work. This is because additional viscous dissipation is caused by the work done on the fluid within the EGJ region by the pressure imposed on the cross-sections

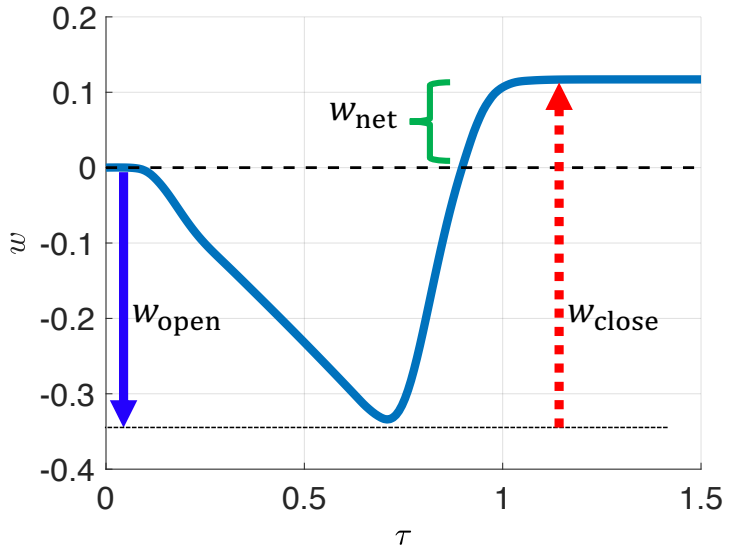

Fig. 9 Graph of the cumulative work done by the EGJ wall on the fluid up to an instant as a function of time. The opening, closing, and net work done by the wall on the fluid area marked.

at the two ends of the EGJ region. This pressure work is equal to the negative of the third term on the RHS of equation (29). Figure 10 has a curve for the third term on the RHS of equation (29).

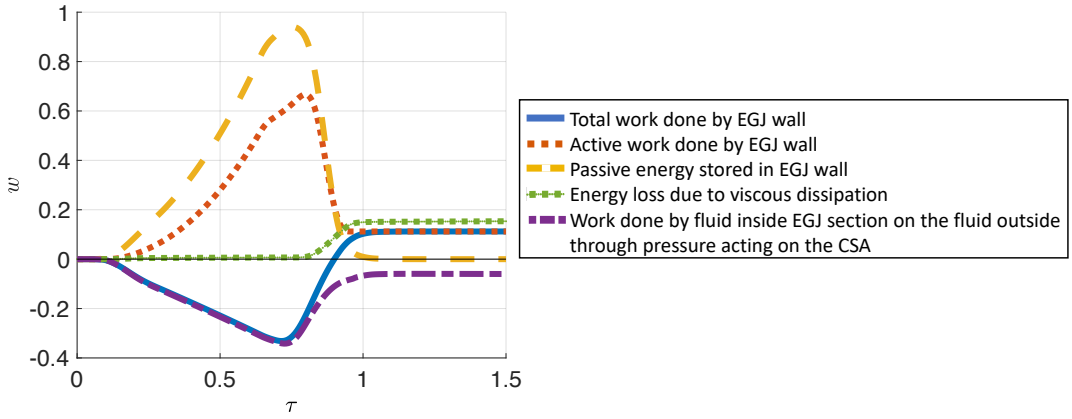

Fig. 10 Plot of the work components from equation (29) evaluated at the EGJ region as they progress over time. Each curve depicts the cumulative work done in the corresponding mode up to a given instant. The total work done by the EGJ wall on the fluid (LHS of equation (22) is also plotted.

3.2.3 Using Work Curves to Identify Loop Type

We now relate the above results to the two loop types identified earlier (figures 6a and 6b). To that end, notice that if the pressure in the EGJ region is nearly uniform (which is a reasonable approximation) then the area under the opening and closing curves in the pressure-area loop graph multiplied by the length of the EGJ is equal to the work done by the fluid to open and close the EGJ walls, respectively.

In the pressure dominant loop, the opening curve is above the closing curve (figure 6a), which implies $|w_{\text{open}}| > |w_{\text{close}}|$. This makes the net work value at the end of the cycle negative in a figure similar to 9.

On the other hand in a tone dominant loop, the opening curve is below the closing curve (figure 6b), which implies $|w_{\text{open}}| < |w_{\text{close}}|$. This makes the net work value at the end of the cycle positive as is the case in figure 9. Hence, we wish to understand what makes $|w_{\text{close}}| > |w_{\text{open}}|$ in a tone dominant loop as opposed to $|w_{\text{close}}| < |w_{\text{open}}|$ in a pressure dominant loop.

During the opening of the EGJ, the fluid (through pressure) does positive work on the EGJ wall, while during closing, the EGJ wall does positive work on the fluid. Hence, if $|w_{\text{close}}| > |w_{\text{open}}|$, the EGJ wall applies more work on the fluid than the fluid exerts on the wall, resulting in a positive net work and a tone dominant loop. In contrast, if $|w_{\text{close}}| < |w_{\text{open}}|$, the fluid applies more work on the EGJ wall than the EGJ wall exerts on the fluid, resulting in a negative net work and a pressure dominant loop. Thus, we wish to identify and explain the key parameters which affect the relation between w_{close} and w_{open}.

Figure 11 displays a plot of only the total, active, and passive work components from figure 10. Five regions are marked on the figure, each representing the magnitude of work done by or stored in the EGJ wall during either opening or closing of the EGJ. The description of each region is presented in table 2. Note that since passive energy fully recovers, the third term also represents the passive energy stored in the EGJ wall during closing.

Table 2: Description of highlighted regions in figure 11

Name	Symbol	Definition
1	$w_{\text{Active,close}}$	Active work done by the EGJ wall on the fluid during closing
2	$w_{\text{Total,close}}$	Total work done by the EGJ wall on the fluid during closing
3	$w_{\text{Passive,open}}$	Passive energy stored in the EGJ wall during opening
4	$w_{\text{Total,open}}$	Total work done by the EGJ wall on the fluid during opening
5	$w_{\text{Active,net}}$	Net active work done by the EGJ wall on the fluid

As figure 11 shows, **(3) = (1) + (4) + (5)**. Thus, **(5) = (3) − (4) − (1)**, or **(5)** $= w_{\text{Passive,open}} - (w_{\text{Passive,open}} - w_{\text{Active,open}}) - w_{\text{Active,close}} = w_{\text{Active,open}} - w_{\text{Active,close}}$. Therefore, the loop type depends on the active opening work relative to the active closing work, which implies that active work is the only work component needed to define the loop type.

Note that the active work is the work required to open the EGJ only by the muscle itself relaxing. However, this can be reduced by helping the EGJ open through mechanical distention (change in the distal pressure). Hence, in discussing what causes w_{close} to be larger or smaller than w_{open}, we must consider the elements which affect distal pressure.

3.3 Key Parameters in Loop Type

Using the simulation results, we conduct a parametric study to examine the leading parameters that dictate the loop type. Out of the eight parameters listed in table 1, only three parameters affect the loop type. These non-dimensional parameters are ψ, β, and γ, each dominated by a different physical property, which are wall stiffness, fluid viscosity, and EGJ relaxation speed, respectively. The rest of the parameters affect the loop quantitatively, such as slightly changing the loop shape or area, but do not contribute to the conversion between the two loop types.

In this section, we discuss the affect of ψ, β, and γ on the loop type through looking at the total, passive and active work done by the EGJ wall. However, it is important to note that γ, which represents the speed of the neurogenic mediated relaxation at the EGJ, is the primary mechanism in clinical FLIP data. Fluid properties and esophageal stiffness are mostly consistent among clinical data. Consequently, they cannot be considered the main explanation for the presence of two loop types.

3.3.1 EGJ Relaxation Speed

Figure 12 presents the work plots and pressure-cross-sectional area loops of two different contraction cycle simulations with the same input parameters ($\beta = 100, \psi = 600$), but the value of γ. Figures 12a and

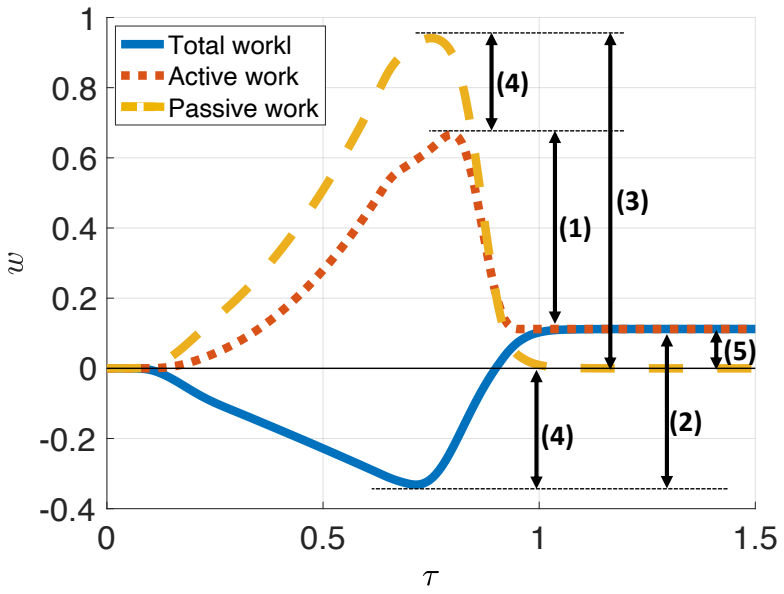

Fig. 11 Plot of the total, active, and passive work components at the EGJ region as they progress over time. The five regions marked on the figure represent the work done by or stored in the EGJ wall during either opening or closing of the EGJ, defined in table 2.

12b display the work curves and pressure-area loop, respectively, for the simulation where the EGJ relaxes quickly ($\gamma = 0.06$). Figures 12c and 12d display the work curves and pressure-area loop, respectively, for the simulation where the EGJ relaxes slowly ($\gamma = 0.6$). As these figures show, EGJ neurogenic mediated relaxation speed alone can change the loop type, with tone dominant loop associated with fast relaxation of the EGJ and pressure dominant loop associated with slow relaxation of the EGJ. Accordingly, when the EGJ relaxes quickly, $|w_{\text{close}}| > |w_{\text{open}}|$, which is equivalent to $|w_{\text{Active,close}}| < |w_{\text{Active,open}}|$, and when the EGJ relaxes slowly, $|w_{\text{close}}| < |w_{\text{open}}|$, which is equivalent to $|w_{\text{Active,close}}| > |w_{\text{Active,open}}|$.

Notice from figures 12a and 12c that $w_{\text{Active,close}}$ is equal in both fast and slow relaxation simulations. This is because all parameters during contraction, including the contraction pattern, are the same in both cases. Thus, the difference in both the resulting loop type and the value of the net total work must originate from the opening active work, where $|w_{\text{Active,open}}|_{\gamma=0.6} < |w_{\text{Active,open}}|_{\gamma=0.06}$. The active work done by the EGJ wall during opening when the EGJ relaxes slowly is less than when the EGJ relaxes quickly ($|w_{\text{Active,open}}|_{\text{slow}} < |w_{\text{Active,open}}|_{\text{fast}}$).

Recall that when the EGJ starts relaxing, the reference area at the EGJ starts increasing such that the actual shape lags the relaxed shape. The active work is the work done by EGJ tone to overcome fluid suction and match the actual shape to the relaxed shape. As previously mentioned, this work can be reduced by helping the EGJ open through mechanical distention by increasing pressure at the EGJ location (distal pressure). In the case of the esophagus, distal pressure increases by a peristaltic wave traveling down the tube length, which takes place in parallel to the active relaxation of the EGJ. Through this pressure increase, the amount of active work exerted by the EGJ wall on the fluid is reduced in two ways. First, it reduces the effect of fluid suction. Second, it increases the cross-sectional area at the EGJ, making the actual EGJ cross-section closer to the reference cross-section.

When the EGJ relaxes quickly, the reference area grows rapidly, but the peristaltic wave has barely traveled, as seen in figure 3b. Consequently, the contribution from pressure increase by the traveling contraction wave is limited, such that the EGJ tone must apply more active work to increase the actual EGJ cross-sectional area to match the fast-increasing reference area. The lack of contribution from mechanical distention in this cases causes $|w_{\text{Active,close}}| < |w_{\text{Active,open}}|$.

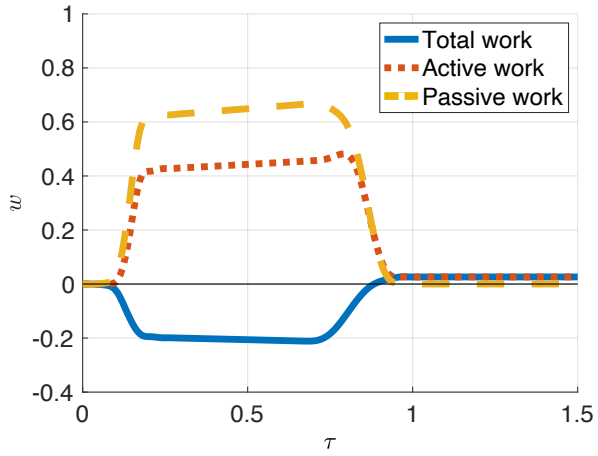

(a) Work curves, $\gamma = 0.06$

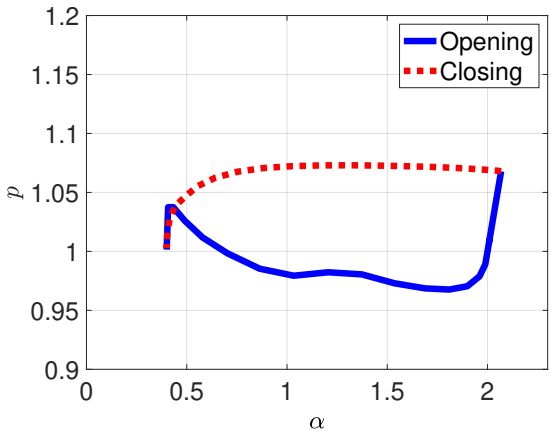

(b) Pressure-area loop at EGJ, $\gamma = 0.06$

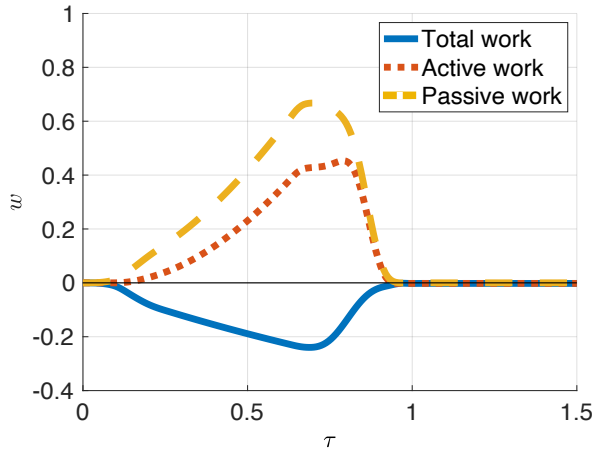

(c) Work curves, $\gamma = 0.6$

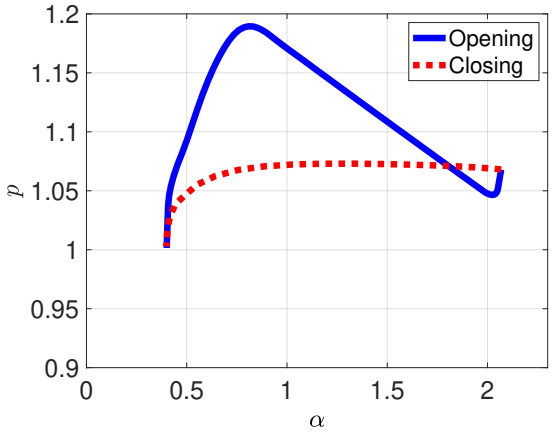

(d) Pressure-area loop at EGJ, $\gamma = 0.6$

Fig. 12 Results of two contraction cycle simulations, differentiated by the implemented γ value. Figures (a) and (c) present the total, passive and active work curves evaluated at the EGJ region as a function of time. Figures (b) and (d) display the corresponding pressure-cross-sectional area plots at the EGJ location throughout the contraction cycle. One simulation results in a tone dominant loop and the other in a pressure dominant loop.

Notice that we only discuss EGJ relaxation speed, ignoring the potential affect of the closing pattern on the resulting loop type. By looking at clinical FLIP recordings of different contraction cycles, it was observed that the active contraction of the EGJ is set by the peristaltic wave traveling into and stopping at the EGJ location, similar to the pattern used in the model above (Acharya et al., 2020; Lin et al., 2013; Carlson et al., 2016). Thus, the speed of the contraction of the EGJ at the end of the contraction cycle depends on the speed of the traveling wave. While we recognize that the speed of the traveling contraction is a parameter in the system that affects the neurally controlled activation function at the EGJ, we argue that relaxation pattern is the more dominant parameter in differentiating loop types. This is because the speed of the traveling contraction does not widely vary across subjects. The wave speed c is a known constant ($c = 1.5 - 3$ cm/s) that was determined by calculating the distance traveled by the contraction wave over time (Kou et al., 2015; Li et al., 1994).

3.3.2 Tube Stiffness

While the the primary mechanism of the emergence of two pressure-cross-sectional area loop types in clinical FLIP data is the EGJ relaxation speed dictated by neurally controlled muscle activation, ψ and β also play a role. For the purpose of completeness as well as obtaining a better understanding of peristaltic flow in a flexible tube, we present the results attained by varying these two parameters. The following section focuses on the affect of stiffness, through changing the value of $\psi = K_e/\rho c^2$, on the resulting loop type.

Figure 13 presents the work plots and pressure-cross-sectional area loops of two different contraction cycle simulations with the same input parameters ($\beta = 100, \gamma = 0.6$), but the value of ψ. Figures 13a and 13b display the work curves and pressure-cross-sectional area loop, respectively, for the simulation where wall stiffness is relatively low ($\psi = 100$). Figures 13c and 13d display the work curves and pressure-cross-sectional area loop, respectively, for the simulation where wall stiffness is relatively high ($\psi = 2,400$). As the figure shows, change in ψ is sufficient to affect the loop type, where high values of ψ are associated with pressure dominant loops (figure 6a) and low values of ψ are associated with tone dominant loops (figure 6b). As expected, figure 13 shows that the tone dominant case displays $|w_{\text{close}}| > |w_{\text{open}}|$, while the pressure dominant case displays $|w_{\text{close}}| < |w_{\text{open}}|$.

(Acharya et al., 2021) and (Elisha et al., 2022) studied the relation between wall stiffness and tube deformation in peristaltic flow through a flexible tube closed on both ends. They revealed that when wall stiffness is high, it resists deformation, so as the wave travels down the tube length, the displaced fluid is forced to flow back through the peristaltic contraction. This is because more energy is needed to expand the tube wall distal to the traveling contraction than the energy needed to overcome flow resistance across the contraction. On the other hand, when stiffness is low, the tube wall distal to the contraction tends to expand to accommodate for the fluid that is being displaced by the traveling peristaltic wave.

With the above knowledge in mind, we can explain the observations attained from figure 13. The lower the stiffness, the more compliant the tube is, and the distal cross-sectional area expands further to accommodate for the displaced fluid. The extended expansion of the distal tube wall means that a large amount of fluid has accumulated at the EGJ location, which increases fluid resistance (Elisha et al., 2022). Hence, when the EGJ starts closing, the resistance is high, and the EGJ tone needs to apply more work on the fluid in order to close. Consequently, we see that $|w_{\text{close}}| > |w_{\text{open}}|$ and a corresponding tone dominant loop. In the second scenario, where tube stiffness is high, the wall resists its expansion so that fluid is more equally distributed along the tube length. Thus, less work is required to contract the EGJ wall than to expand it, which implies $|w_{\text{close}}| < |w_{\text{open}}|$ and the corresponding loop is a pressure dominant loop.

3.3.3 Fluid Viscosity

We can do a similar analysis as in section 3.3.2, but this time, we focus on parameter $\beta = 8\pi\mu L/\rho A_o c$. Figure 14 presents the work plots and pressure area loops of two different contraction cycle simulations of the same input parameters ($\psi = 100, \gamma = 0.6$), but the value of β. In the work plot and loop in figures 14a and 14b, respectively, $\beta = 100$, and in the work plot and loop in figures 14c and 14d, respectively, $\beta = 1,000$. As the figure shows, change in β is sufficient to affect the loop type, where low values of β are associated with pressure dominant loops (figure 6a) and high values of β are associated with tone dominant loops (figure 6b). Since the parameter β is dominated by the fluid viscosity (μ), varying the value of β can be looked at as varying fluid viscosity. Hence, pressure dominant loop is associated with low fluid viscosity and tone dominant loop is associated with high fluid viscosity. As predicted by previous discussions, figure 14 shows that the tone dominant case displays $|w_{\text{close}}| > |w_{\text{open}}|$, while the pressure dominant case displays $|w_{\text{close}}| < |w_{\text{open}}|$.

In order to explain this observation, we refer back to the conclusions obtained by (Acharya et al., 2021) and (Elisha et al., 2022). As long as the traveling peristaltic wave remains contracted, the fluid resistance increases with the increase in fluid viscosity. If the resistance to flow is high, less energy is needed to expand the tube wall distal to the traveling contraction than the energy needed to overcome flow resistance across the contraction. Thus, high viscosity results in cross-sectional area expansion at the distal end, causing fluid to accumulate at the EGJ location. Both the fluid accumulation at the EGJ location and the high

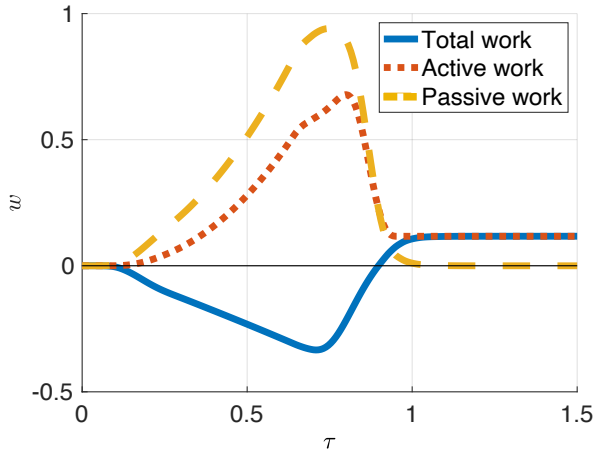

(a) Work curves, $\psi = 100$

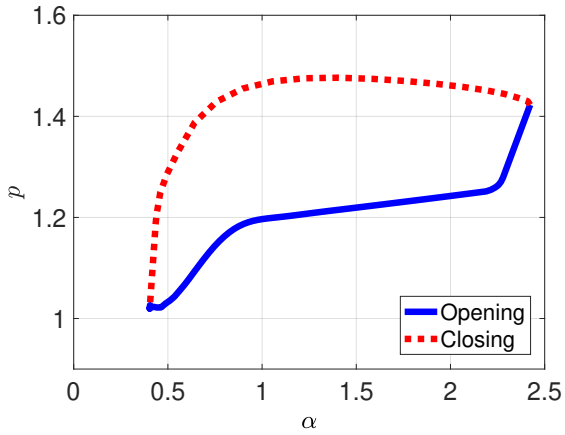

(b) Pressure-area loop at EGJ, $\psi = 100$

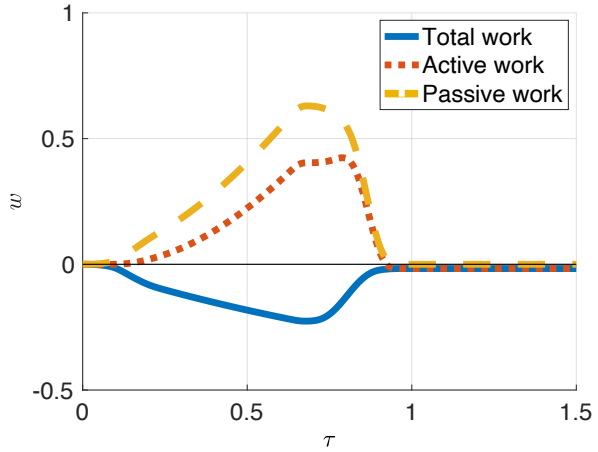

(c) Work curves, $\psi = 2,400$

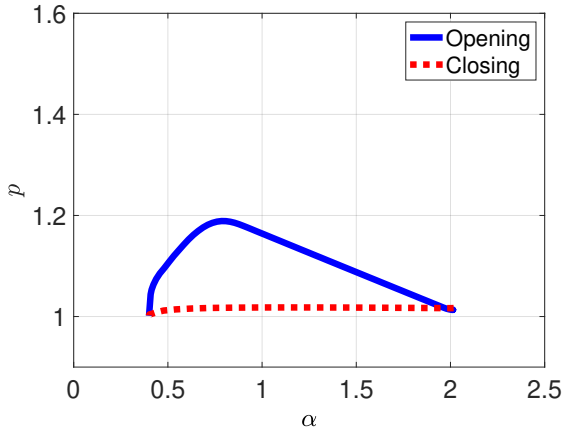

(d) Pressure-area loop at EGJ, $\psi = 2,400$

Fig. 13 Results of two contraction cycle simulations, differentiated by the implemented ψ value. Figures (a) and (c) present the total, passive and active work curves evaluated at the EGJ region as a function of time. Figures (b) and (d) display the corresponding pressure-cross-sectional area plots at the EGJ location throughout the contraction cycle. One simulation results in a tone dominant loop and the other in a pressure dominant loop.

flow resistance caused by increasing viscosity requires large amount of work to close the EGJ, such that $|w_{\text{close}}| > |w_{\text{open}}|$ is observed and a tone dominant loop emerges. On the other hand, when the viscosity is low, the flow resistance is low, and it is favorable for the system to allow back flow through the contraction than to expand the tube walls to accommodate the displaced fluid. Therefore, it appears that less work in needed to close the EGJ than to open it. In this case, $|w_{\text{close}}| < |w_{\text{open}}|$ and a pressure dominant loop emerges.

3.4 Application to Clinical Data

Since the fluid viscosity and esophagus stiffness are generally the same among subjects, the results presented in section 3.3 indicate that the main parameter causing the difference in the pressure-area loops is neuromuscular. We wish to examine this conclusion by directly calculating and plotting the work curves of

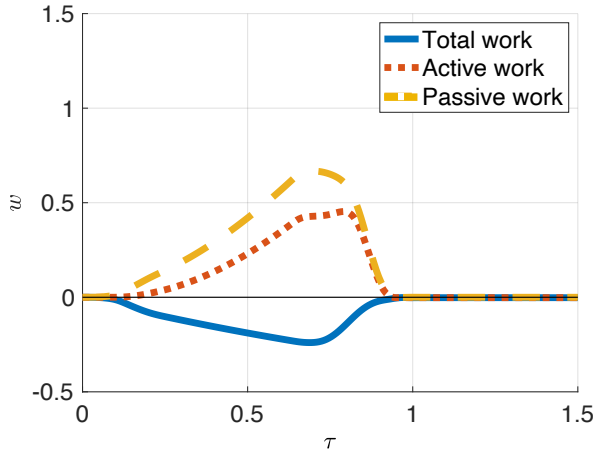

(a) Work curves, $\beta = 100$

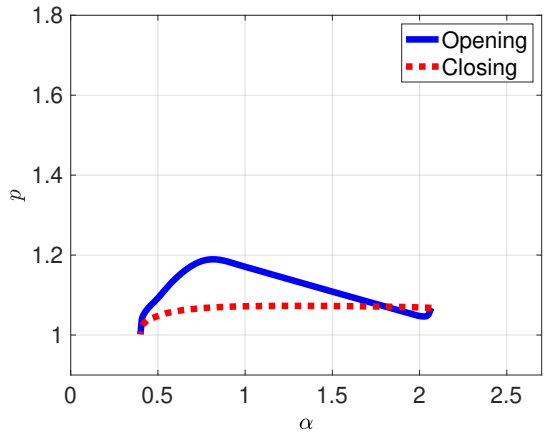

(b) Pressure-area loop at EGJ, $\beta = 100$

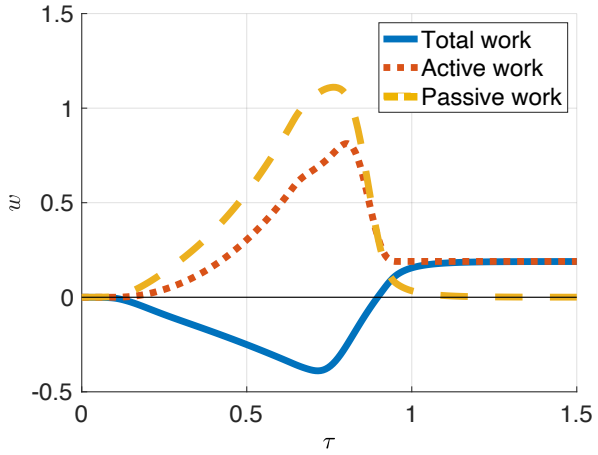

(c) Work curves, $\beta = 1,000$

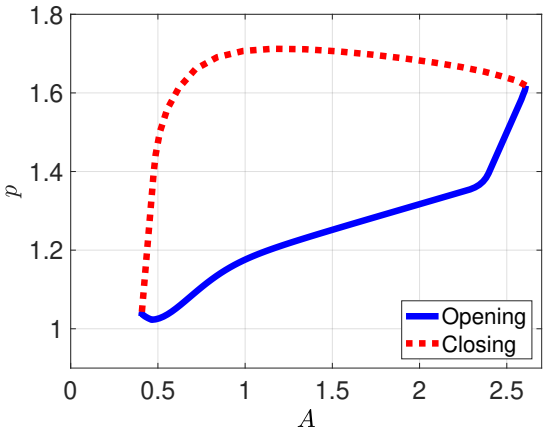

(d) Pressure-area loop at EGJ, $\beta = 1,000$

Fig. 14 Results of two contraction cycle simulations, differentiated by the implemented β value. Figures (a) and (c) present the total, passive and active work curves evaluated at the EGJ region as a function of time. Figures (b) and (d) display the corresponding pressure-cross-sectional area plots at the EGJ location throughout the contraction cycle. One simulation results in a tone dominant loop and the other in a pressure dominant loop.

clinical data alongside their pressure-cross-sectional area loops. For this calculation, the cross-sectional area values are direct FLIP readings. The activation function ($\theta(x,t)$), P_o, and the ratio K_e/A_o are calculated as proposed by Halder et al. (2021) using the momentum equation in equation (2). The fluid properties are density $\rho = 1000$ kg/m^3 and viscosity $\mu = 0.001$ Pa $\cdot$ s (Kou et al., 2015).

Figure 15 presents the graph of the total work done by the EGJ wall (left) alongside the corresponding pressure-area loop at the EGJ location (right) of a clinical contraction cycle. As the figure shows, the overall pattern of the work curve and its relation to the loop is the same as in the simulations, as observed by highlighting five instances on the two figures. During EGJ opening, the total work done by the EGJ wall on the fluid decreases while the pressure and cross-sectional area increase. At point 3, the EGJ is fully open, so that the pressure and cross-sectional area are maximal, while the cumulative total work is at its minimum. Once the EGJ starts to close, it does positive work on the fluid so the total work done by the EGJ wall on

the fluid increases while pressure and cross-sectional area decrease. The value of the net work (at point 5) is negative, a characteristic of a pressure dominant loop, which is exactly the loop type corresponding to this work plot. Hence, we can explain the clinical work curve based on the conclusions from the simulation results discussed in section 3.2.2.

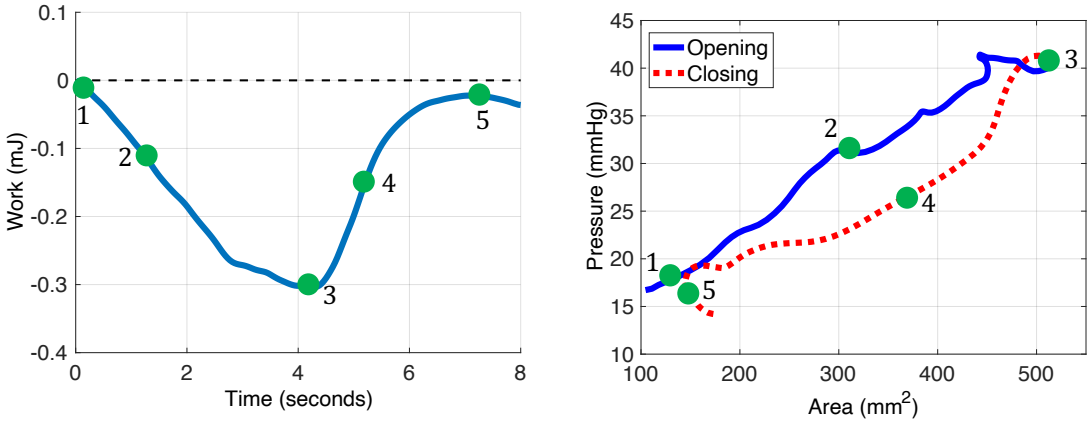

Fig. 15 Plots of the total work done by the EGJ wall of the fluid (left) and the corresponding pressure-cross-sectional area plot at the EGJ location (right), extracted from clinical FLIP reading of a single contraction cycle.

Figure 16 presents the work curves and pressure-cross-sectional area plots of two contraction cycles, extracted from clinical FLIP data. Figure 16a presents a pressure dominant loop and figure 16b presents a tone dominant loop. As the figure shows, the net work done by the EGJ wall is positive for the tone dominant loop and negative for pressure dominant loop. In addition, the figure shows that the passive and active work curves display similar trends to the ones obtained by the simulations. The most important observation however can be extracted by highlighting one instance in the contraction cycle, which correspond to when the EGJ is fully open. As the figure shows, the full opening for the tone dominant loop occurs earlier in the cycle than for the pressure dominant loop. As concluded in section 3.3.1, this is the parameter differentiating the two loops. The slower the opening, the higher the contribution of mechanical distention, and the less active work the EGJ needs to exert on the fluid in order to open.

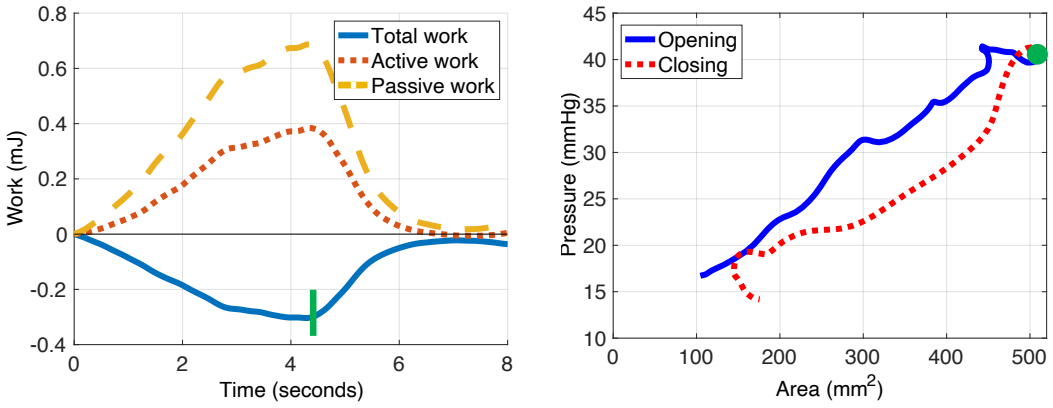

(a) Plot of the total, active and passive work evaluated at the EGJ (left) and the corresponding pressure cross-sectional area plot at the EGJ location (right), extracted from clinical FLIP reading of a single contraction cycle. This contraction cycle exhibiting a pressure dominant loop.

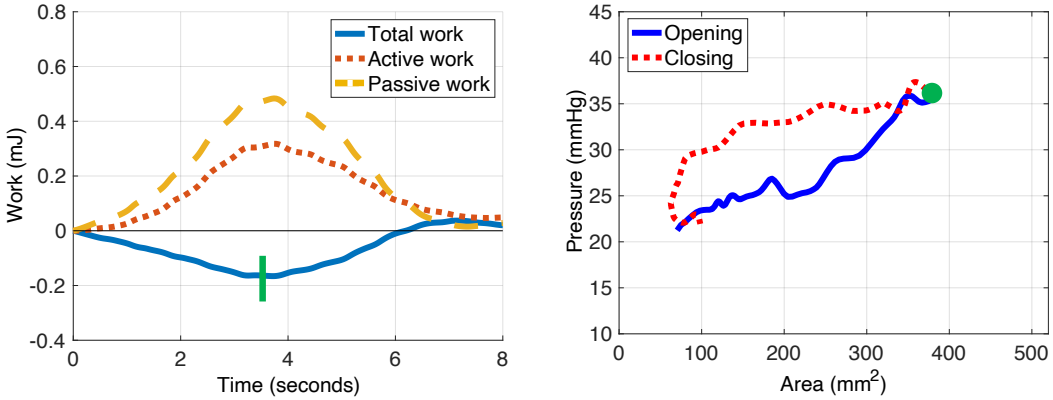

(b) Plot of the total, active and passive work evaluated at the EGJ (left) and the corresponding pressure cross-sectional area plot at the EGJ location (right), extracted from clinical FLIP reading of a single contraction cycle. This contraction cycle exhibiting a tone dominant loop.

Fig. 16 Comparing work plots and pressure-area loops of two clinical contraction cycles. The figure at the top corresponds to contraction cycle with pressure dominant loop whereas the figure at the bottom figure corresponds to contraction cycle with tone dominant loop.

4 Conclusion

The main objective of this study was to get a better understanding of the opening and closing mechanism of the EGJ during a contraction cycle. Post processing clinical FLIP data led to identifying two major pressure-cross-sectional area loop types. The tone dominant loop, identified as the loop wherein the closing curve is above the opening curve, is characterized by low esophageal stiffness, high fluid viscosity, and rapid relaxation of EGJ tone. In contraction cycles with tone dominant loop, the net work done by the EGJ wall

throughout the contraction cycle is positive, which implies that the EGJ wall applies more work on the fluid than the pressure in the fluid applies on the EGJ wall. The pressure dominant loop, identified as the loop where the opening curve is above the closing curve, is characterized by high esophageal stiffness, low fluid viscosity, and slow relaxation of the EGJ tone. In contraction cycles with a pressure dominant loop, the net work done by the EGJ wall throughout the contraction cycle is negative, which implies that the pressure in the fluid applies more work on the EGJ wall than the EGJ wall applies on the fluid.

In this work, we dissected a clinical phenomenon into its physical parameters. Hence, rather than examining the pressure-cross-sectional area loops at the EGJ as a function of time, we aimed to get a better understanding of the EGJ function through mechanics, and therefore, identify the leading parameter that dictates the loop shape. From the simulations and parametric study presented in this writing, we concluded that the dominant reason for the presence of two pressure-area loop types at the EGJ during a contraction cycle is controlled by neuromuscular mechanism. The activation function applied by the esophageal muscles dictates the loop type rather than fluid or material properties. Moreover, this work is another example of a fundamental study which helps us explain clinical observations. While the pressure-area loops at the EGJ are generally viewed as noisy, they are shown to be the result of a clear, repeating pattern that we can physically explain. The conclusions of this work give us a better view into the physical held of the system, and a deeper understanding of the EGJ function. These insights bring us a step closer to identifying the underlying conditions that cause EGJ dysfunction.

Declarations

Ethical approval

The study protocol was approved by the Northwestern University Institutional Review Board. Informed consent was obtained from all subjects; subjects were paid for their participation.

Authors' contribution

G.E., wrote the main manuscript text and prepared all the figures; G.E., S.H., and S.A., wrote the code; N.A.P., G.E., S.H., and S.A., developed the mathematical formulation; D.A.C., and W.K., contributed to data acquisition; G.E., S.H., W.K., D.A.C., N.A.P., P.J.K., J.E.P., interpreted results of calculations; J.E.P., P.J.K., and N.A.P., contributed to obtaining funding, critical revision of the manuscript and final approval.

Funding

This work was funded by the by the National Institutes of Health (NIDDK grants DK079902 & DK117824 and NIDDK grants DK079902), and National Science Foundation (OAC grants 1450374 & 1931372)

Conflict of interest

Peter J. Kahrilas, and John E. Pandolfino hold shared intellectual property rights and ownership surrounding FLIP panometry systems, methods, and apparatus with Medtronic Inc.

Dustin A. Carlson: Medtronic (Speaking, Consulting)

Wenjun Kou: Crospon, Inc. (Consulting)

Peter J. Kahrilas: Ironwood (Consulting), Reckitt (Consulting), Johnson & Johnson (Consulting)

John E. Pandolfino: Crospon, Inc (stock options), Given Imaging (Consultant, Grant, Speaking), Sandhill Scientific (Consulting, Speaking), Takeda (Speaking), Astra Zeneca (Speaking), Medtronic (Speaking, Consulting), Torax (Speaking, Consulting), Ironwood (Consulting), Impleo (Grant)

G. Elisha, S. Halder, S. Acharya, N.A. Patankar: None

Availability of data and materials

Not applicable

References

L. Abrahao Jr, V. Bhargava, A. Babaei, A. Ho, and R. K. Mittal. Swallow induces a peristaltic wave of distension that marches in front of the peristaltic wave of contraction. *Neurogastroenterology & Motility*, 23 (3):201–e110, 2011. doi: 10.1111/j.1365-2982.2010.01624.x. URL https://onlinelibrary.wiley.com/doi/abs/10.1111/j.1365-2982.2010.01624.x.

Shashank Acharya, Sourav Halder, Dustin A Carlson, Wenjun Kou, Peter J. Kahrilas, John E Pandolfino, and Neelesh A Patankar. Assessment of esophageal body peristaltic work using functional lumen imaging probe panometry. *American Journal of Physiology-Gastrointestinal and Liver Physiology*, 2020. doi: 10.1152/ajpgi.00324.2020. URL https://doi.org/10.1152/ajpgi.00324.2020. PMID: 33174457.

Shashank Acharya, Wenjun Kou, Sourav Halder, Dustin A. Carlson, Peter J. Kahrilas, John E. Pandolfino, and Neelesh A. Patankar. Pumping patterns and work done during peristalsis in finite-length elastic tubes. *Journal of Biomechanical Engineering*, 143(7), Mar 2021. ISSN 1528-8951. doi: 10.1115/1.4050284. URL http://dx.doi.org/10.1115/1.4050284.

Guy E. Boeckxstaens, Giovanni Zaninotto, and Joel E. Richter. Achalasia. *The Lancet*, 393(9911):83–93, January 2014. doi: 10.1016/S0140-6736(13)60651-0. URL https://doi.org/10.1016/S0140-6736(13)60651-0.

Thomas T. Bringley, Stephen Childress, Nicolas Vandenberghe, and Jun Zhang. An experimental investigation and a simple model of a valveless pump. *Physics of Fluids*, 20(3):033602, March 2008. doi: 10.1063/1.2890790. URL https://doi.org/10.1063/1.2890790.

Dustin A. Carlson, Zhiyue Lin, Peter J. Kahrilas, Joel Sternbach, Erica N. Donnan, Laurel Friesen, Zoe Listernick, Benjamin Mogni, and John E. Pandolfino. The functional lumen imaging probe detects esophageal contractility not observed with manometry in patients with achalasia. *Gastroenterology*, 149(7):1742–1751, December 2015. doi: 10.1053/j.gastro.2015.08.005. URL https://doi.org/10.1053/j.gastro.2015.08.005.

Dustin A. Carlson, Peter J. Kahrilas, Zhiyue Lin, Ikuo Hirano, Nirmala Gonsalves, Zoe Listernick, Katherine Ritter, Michael Tye, Fraukje A. Ponds, Ian Wong, and John E. Pandolfino. Evaluation of esophageal motility utilizing the functional lumen imaging probe. *American Journal of Gastroenterology*, 111(12): 1726–1735, December 2016. doi: 10.1038/ajg.2016.454. URL https://doi.org/10.1038/ajg.2016.454.

Dustin A Carlson, Wenjun Kou, Zhiyue Lin, Monique Hinchcliff, Anjali Thakrar, Sophia Falmagne, Jacqueline Prescott, Emily Dorian, Peter J Kahrilas, and John E Pandolfino. Normal values of esophageal distensibility and distension-induced contractility measured by functional luminal imaging probe panometry. *Clinical Gastroenterology and Hepatology*, 17(4):674–681, 2019. doi: 10.1016/j.cgh.2018.07.042.

Dustin A. Carlson, Alexandra J. Baumann, Jacqueline E. Prescott, Erica N. Donnan, Rena Yadlapati, Abraham Khan, C Prakash Gyawali, Wenjun Kou, Peter J. Kahrilas, and John E. Pandolfino. Validation of secondary peristalsis classification using flip panometry in 741 subjects undergoing manometry. *Neurogastroenterology and motility*, 34(1):e14192, June 2021a. doi: 10.1111/nmo.14192. URL https://doi.org/10.1111/nmo.14192.

Dustin A. Carlson, C. Prakash Gyawali, Abraham Khan, Yadlapati, Joan Chen, Reena V. Chokshi, John O. Clarke, Jose M. Garza, Anand S. Jain, Philip Katz, Vani Konda, Kristle Lynch, Felice H. Schnoll-Sussman, Stuart J. Spechler, Marcelo F. Vela, Jacqueline E Prescott, Alexandra J. Baumann, Erica N. Donnan, Wenjun Kou, Peter J. Kahrilas, and John E. Pandolfino. Classifying esophageal motility by flip panometry:

A study of 722 subjects with manometry. *American Journal of Gastroenterology*, October 2021b. doi: 10.14309/ajg.0000000000001532. URL https://doi.org/10.14309/ajg.0000000000001532.

Jefferey Crist, Jaswant S. Gidda, and Raj K. Goyal. Intramural mechanism of esophageal peristalsis: roles of cholinergic and noncholinergic nerves. *Proceedings of the National Academy of Sciences of the United States of America*, 81(11):3595—-3599, June 1984. doi: 10.1073/pnas.81.11.3595. URL https://doi.org/10.1073/pnas.81.11.3595.

Alexander J Eckardt and Volker F Eckardt. Current clinical approach to achalasia. *World journal of gastroenterology*, 15(32):3969–3975, August 2009. doi: 10.3748/wjg.15.3969. URL https://doi.org/10.3748/wjg.15.3969.

Guy Elisha, Shashank Acharya, Sourav Halder, Dustin A. Carlson, Wenjun Kou, Peter J. Kahrilas, John E. Pandolfino, and Neelesh A. Patankar. Peristaltic regimes in esophageal transport. *Biomechanics and Modeling in Mechanobiology*, November 2022. doi: 10.1007/s10237-022-01625-x. URL https://doi.org/10.1007/s10237-022-01625-x.

Raj K. Goyal and Arun Chaudhury. Physiology of normal esophageal motility. *Journal of clinical gastroenterology*, 42(5):610—-619, August 2008. doi: 10.1097/MCG.0b013e31816b444d. URL https://doi.org/10.1097/MCG.0b013e31816b444d.

Hans Gregersen and Kar Man Lo. What is the future of impedance planimetry in gastroenterology? *Neurogastroenterology and motility*, 24(2):166–181, April 2018. doi: 10.5056/jnm18013. URL https://doi.org/10.5056/jnm18013.

Sourav Halder, Shashank Acharya, Wenjun Kou, Peter J. Kahrilas, John E. Pandolfino, and Neelesh A. Patankar. Mechanics informed fluoroscopy of esophageal transport. *Biomechanics and Modeling in Mechanobiology*, 20(3), Jun 2021. ISSN 1617-7940. doi: 10.1007/s10237. URL https://doi.org/10.1007/s10237-021-01420-0.

Peter J. Kahrilas. Gastroesophageal reflux disease. *The New England journal of medicine*, 359(16):1700–1707, October 2008. doi: 10.1056/NEJMcp0804684. URL https://doi.org/10.1056/NEJMcp0804684.

Wenjun Kou, John E. Pandolfino, Peter J. Kahrilas, and Neelesh A. Patankar. Simulation studies of circular muscle contraction, longitudinal muscle shortening, and their coordination in esophageal transport. *American Journal of Physiology-Gastrointestinal and Liver Physiology*, 309(4):G238–G247, August 2015. doi: 10.1152/ajpgi.00058.2015. URL https://doi.org/10.1152/ajpgi.00058.2015.

Monika A. Kwiatek, John E. Pandolfino, Ikuo Hirano, and Peter J. Kahrilas. Esophagogastric junction distensibility assessed with an endoscopic functional luminal imaging probe (endoflip). *Gastrointestinal endoscopy*, 72(2):272–278, August 2010. doi: 10.1016/j.gie.2010.01.069. URL https://doi.org/10.1016/j.gie.2010.01.069.

Monika A. Kwiatek, Ikuo Hirano, Peter J. Kahrilas, Jami Rothe, Daniel Luger, and John E. Pandolfino. Mechanical properties of the esophagus in eosinophilic esophagitis. *Gastroenterology*, 140(1):82–90, January 2011. doi: 10.1053/j.gastro.2010.09.037. URL https://doi.org/10.1053/j.gastro.2010.09.037.

Meijing Li, James G. Brasseur, and Wylie J. Dodds. Analyses of normal and abnormal esophageal transport using computer simulations. *American Journal of Physiology - Gastrointestinal and Liver Physiology*, 266 (4):525–543, April 1994. doi: 10.1152/ajpgi.1994.266.4.G525. URL https://doi.org/10.1152/ajpgi.1994.266.4.G525.

Zhiyue Lin, Peter J. Kahrilas, Yinglian Xiao, Frederic Nicodeme, Nirmala Gonsalves, Ikuo Hirano, and John E. Pandolfino. Functional luminal imaging probe topography: an improved method for characterizing esophageal distensibility in eosinophilic esophagitis. *Therapeutic Advances in Gastroenterology*, 6(2):97–107, March 2013. doi: 10.1177/1756283X12470017. URL https://doi.org/10.1177/1756283X12470017.

Christos G. Manopoulos, Demetri S. Mathioulakis, and Sokrates G. Tsangaris. One-dimensional model of valveless pumping in a closed loop and a numerical solution. *Physics of Fluids*, 18(1):017106, January 2006. doi: 10.1063/1.2165780. URL https://doi.org/10.1063/1.2165780.

Ravinder K. Mittal. Regulation and dysregulation of esophageal peristalsis by the integrated function of circular and longitudinal muscle layers in health and disease. *American Journal of Physiology-Gastrointestinal and Liver Physiology*, 311(3):G431–G443, September 2016. doi: 10.1152/ajpgi.00182.2016. URL https://doi.org/10.1152/ajpgi.00182.2016.

Ravinder K. Mittal and David H. Balaban. The esophagogastric junction. *The New England Journal of Medicine*, 336(13):924–932, March 1997. doi: 10.1056/NEJM199703273361306. URL https://doi.org/10.1056/NEJM199703273361306.

Taher I. Omari, Lukasz Wiklendt, Philip Dinning, Marcello Costa, Nathalie Rommel, and Charles Cock. Upper esophageal sphincter mechanical states analysis: a novel methodology to describe ues relaxation and opening. *Frontiers in Systems Neuroscience*, 8:241, January 2015. doi: 10.3389/fnsys.2014.00241. URL https://doi.org/10.3389/fnsys.2014.00241.

Taher I Omari, Corinne A Jones, Michael J Hammer, Charles Cock, Philip Dinning, Lukasz Wiklendt, Marcello Costa, and Timothy M McCulloch. Predicting the activation states of the muscles governing upper esophageal sphincter relaxation and opening. *American Journal of Physiology-Gastrointestinal and Liver Physiology*, 310(6):G359–G366, 2016. doi: 10.1152/ajpgi.00388.2015.

J.T. Ottesen. Valveless pumping in a fluid-filled closed elastic tube-system: one-dimensional theory with experimental validation. *Journal of Mathematical Biology*, 46(4):309–332, April 2003. doi: 10.1007/s00285-002-0179-1. URL https://doi.org/10.1007/s00285-002-0179-1.

John E. Pandolfino, Guoxiang Shi, Brian Trueworthy, and Peter J. Kahrilas. Esophagogastric junction opening during relaxation distinguishes nonhernia reflux patients, hernia patients, and normal subjects. *Gastroenterology*, 125(4):1018–1024, October 2003. doi: 10.1016/S0016-5085(03)01210-1. URL https://doi.org/10.1016/S0016-5085(03)01210-1.

Nicholas J. Shaheen, Richard A. Hansen, Douglas R. Morgan, Lisa M. Gangarosa, Yehuda Ringel, Michelle T. Thiny, Mark W. Russo, and Robert S. Sandler. The burden of gastrointestinal and liver diseases. *American Journal of Gastroenterology*, 101(9):2128–2138, August 2010. doi: 10.1111/j.1572-0241.2006.00723.x. URL https://doi.org/10.1111/j.1572-0241.2006.00723.x.

Joseph R Triggs, Dustin A Carlson, Claire Beveridge, Wenjun Kou, Peter J Kahrilas, and John E Pandolfino. Functional luminal imaging probe panometry identifies achalasia-type esophagogastric junction outflow obstruction. *Clinical Gastroenterology and Hepatology*, 18(10):2209–2217, 2020. doi: 10.1016/j.cgh.2019.11.037.

Xiaofei Wang, Jose-Maria Fullana, and Pierre-Yves Lagrée. Verification and comparison of four numerical schemes for a 1d viscoelastic blood flow model. *Computer Methods in Biomechanics and Biomedical Engineering*, 18(15):1704–1725, August 2014. doi: 10.1080/10255842.2014.948428. URL https://doi.org/10.1080/10255842.2014.948428.

R. J. Whittaker, M. Heil, O. E. Jensen, and S. L. Waters. A rational derivation of a tube law from shell theory. *The Quarterly Journal of Mechanics and Applied Mathematics*, 63(4):465–496, August 2010. doi: 10.1093/qjmam/hbq020. URL https://doi.org/10.1093/qjmam/hbq020.

Ali Zifan, Ravinder K. Mittal, David C. Kunkel, Jessica Swartz, Garrett Barr, , and Lori J. Tuttle. Loop analysis of the anal sphincter complex in fecal incontinent patients using functional luminal imaging probe. *American journal of physiology: Gastrointestinal and liver physiology*, 318(1):G66–G76, November 2019. doi: 10.1152/ajpgi.00164.2019. URL https://doi.org/10.1152/ajpgi.00164.2019.